Special Report 76-4

CRREL

CREEP THEORY FOR A FLOATING ICE SHEET

June 1976

Donald E. Nevel

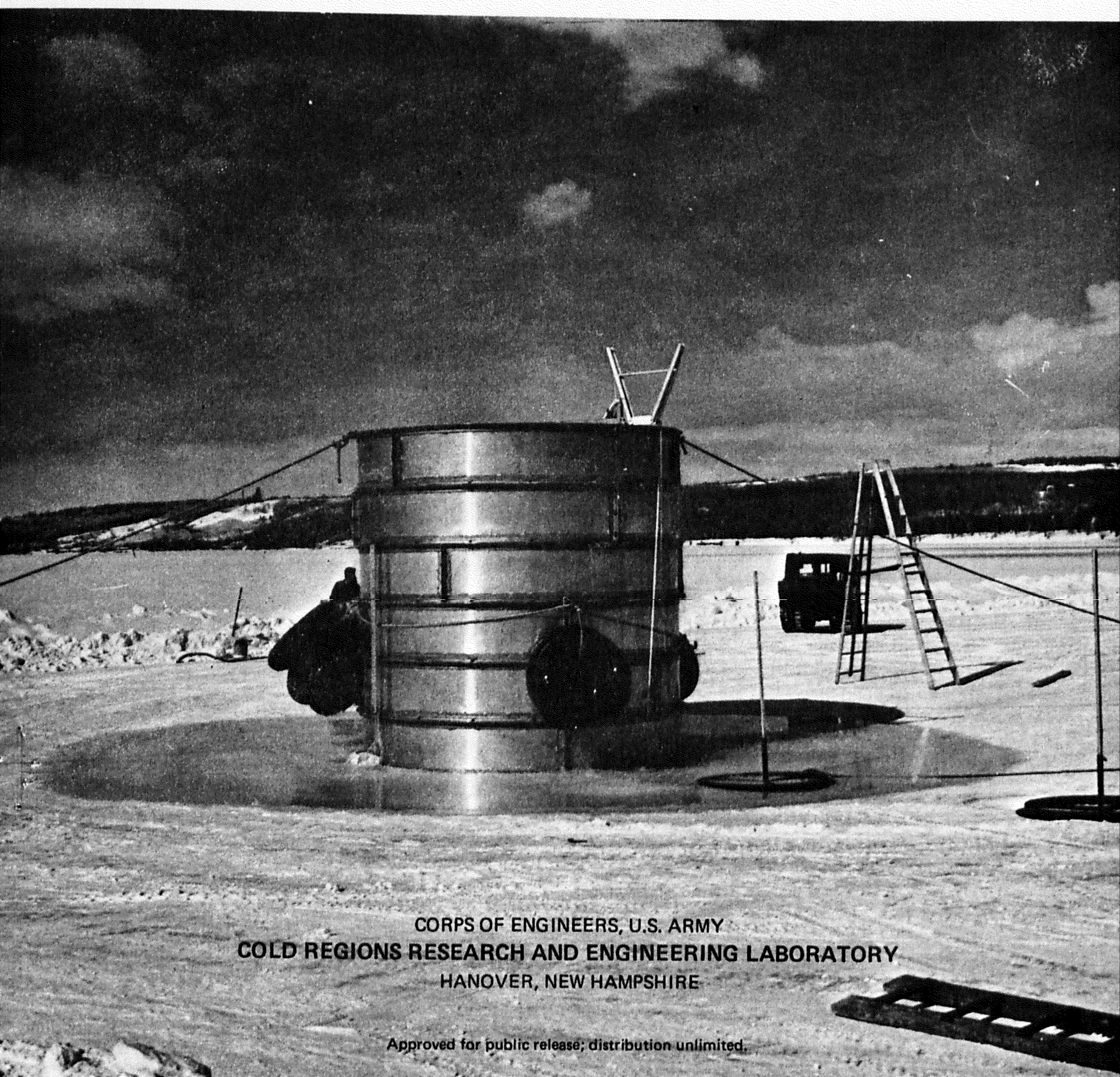

CORPS OF ENGINEERS, U.S. ARMY
COLD REGIONS RESEARCH AND ENGINEERING LABORATORY
HANOVER, NEW HAMPSHIRE

Cover: Floating ice sheet creep test. (Photograph by Guenther Frankenstein.)

Unclassified

SECURITY CLASSIFICATION OF THIS PAGE *(When Data Entered)*

REPORT DOCUMENTATION PAGE

READ INSTRUCTIONS BEFORE COMPLETING FORM

1. REPORT NUMBER Special Report 76-4	2. GOVT ACCESSION NO.
3. RECIPIENT'S CATALOG NUMBER	
4. TITLE *(and Subtitle)* CREEP THEORY FOR A FLOATING ICE SHEET	5. TYPE OF REPORT & PERIOD COVERED
	6. PERFORMING ORG. REPORT NUMBER
7. AUTHOR(s) Donald E. Nevel	8. CONTRACT OR GRANT NUMBER(s)
9. PERFORMING ORGANIZATION NAME AND ADDRESS U.S. Army Cold Regions Research and Engineering Laboratory Hanover, New Hampshire 03755	10. PROGRAM ELEMENT, PROJECT, TASK AREA & WORK UNIT NUMBERS
11. CONTROLLING OFFICE NAME AND ADDRESS U.S. Army Cold Regions Research and Engineering Laboratory Hanover, New Hampshire 03755	12. REPORT DATE June 1976
	13 NUMBER OF PAGES 112
14. MONITORING AGENCY NAME & ADDRESS*(if different from Controlling Office)*	15. SECURITY CLASS. *(of this report)* Unclassified
	15a. DECLASSIFICATION/DOWNGRADING SCHEDULE

16. DISTRIBUTION STATEMENT *(of this Report)*

Approved for public release; distribution unlimited.

17. DISTRIBUTION STATEMENT *(of the abstract entered in Block 20, if different from Report)*

18. SUPPLEMENTARY NOTES

19. KEY WORDS *(Continue on reverse side if necessary and identify by block number)*

Creep
Failure
Ice
Load requirements
Plates

20. ABSTRACT *(Continue on reverse side if necessary and identify by block number)*

The problem investigated in this thesis is the prediction of the deflection and stresses in a floating ice sheet under loads which act over a long period of time. This problem is currently important for oil exploration offshore in the Arctic. A review of analytical methods for predicting the bearing capacity of an ice sheet is given. The problem is formulated by assuming the ice is isotropic with a constant Poisson's ratio. The shear modulus is assumed to obey a linear viscoelastic model. The specific model selected is a series of one Maxwell model and two Voigt models. One of the Voigt models has a negative spring constant which produces tertiary creep. The ice model exhibits a primary, secondary, and tertiary creep response, similar to that observed in uniaxial creep tests of ice. The material properties

DD FORM 1 JAN 73 1473 EDITION OF 1 NOV 65 IS OBSOLETE

Unclassified

SECURITY CLASSIFICATION OF THIS PAGE *(When Data Entered)*

20. Abstract (cont'd)

in the viscoelastic model may be a function of the vertical position in the ice sheet, but all these material properties must be proportional to the same function of position. Using the thin-plate theory for the floating ice sheet, the solution is obtained for the deflection and stresses in the ice sheet for primary, secondary, and tertiary creep regions. It is then shown that for a load that is not distributed over a large area, the time-dependent part of the deflection and stresses is relatively independent of the load's distribution. For the elastic case, the stress significantly depends upon the load's distribution. Results are given for the deflection and stresses as a function of time and distance from the load. The maximum deflection and stresses occur at the center of the load. At this point the deflection increases with time, while the stresses decrease; i.e., the stresses relax.

EXTENDED ABSTRACT

The problem investigated in this report is the prediction of the deflection and stresses in a floating ice sheet under loads which act over a long period of time. This problem is currently important because oil companies wish to use the arctic sea ice as a floating platform for offshore exploratory operations. Loads from one to two million pounds are anticipated for a three-to-four month period.

A review of analytical methods for predicting the bearing capacity of an ice sheet is given. In order to formulate the problem, the ice is assumed to be isotropic with a constant Poisson's ratio. The shear modulus is assumed to obey a linear viscoelastic model. The specific model selected is a series of one Maxwell model and two Voigt models. One of the Voigt models has a negative spring constant which produces tertiary creep. The ice model exhibits a primary, secondary, and tertiary creep response, similar to that observed in uniaxial creep tests of ice. The material properties in the viscoelastic model may be a function of the vertical position in the ice sheet, but all these material properties must be proportional to the same function of position.

Using the thin-plate theory for the floating ice sheet, the solution is obtained by using a two-sided Laplace transform in time and a Hankel transform on the radial distance from the load center. Equations are developed for the deflection and stresses in the ice sheet for primary,

secondary, and tertiary creep regions. It is then shown that for a load that is not distributed over a large area, the time-dependent part of the deflection and stresses is relatively independent of the load's distribution. For the elastic case, the stress significantly depends upon the load's distribution.

Results in tabular and graphical form are given for the deflection and stresses as a function of time and distance from the load. The maximum deflection and stresses occur at the center of the load. At this point the solution simplifies, and for secondary creep becomes

$$w = \frac{P}{8k\ell^2} \; {}_1F_1(-0.5, 1, -T)$$

$$\sigma = \frac{-3P(1+\nu)}{8\pi h^2} \left[E_1(T) + \gamma + \log T\right] + \sigma^o$$

where

- w is the vertical deflection,
- P is the load,
- k is the unit weight of water,
- ℓ^4 is the flexural rigidity of the ice plate divided by k,
- ${}_1F_1$ is the confluent hypergeometric function,
- T is dimensionless time, $E_o\, t/\eta_o$
- t is the time,
- E_o is an elastic constant,
- η_o is a viscous constant,
- σ is the stress,
- σ^o is the elastic stress,
- ν is Poisson's ratio,
- h is the ice thickness,
- E_1 is an exponential integral function,
- γ is Euler's constant.

These equations show that at the load, the deflection increases with time while the stresses decrease; i.e., the stresses relax. This means the maximum tensile stress occurs at time zero.

The usual failure criterion for ice is to limit the maximum tensile stress. If this criterion is used, the ice sheet should fail at time zero, or not at all. However, observations have shown that the ice sheet can fail after sustaining a load for a period of time. An explanation for this discrepancy is that the creep process affects the tensile strength of the ice. There is limited observation which supports this concept.

A discussion of the material properties available from creep tests on floating ice sheets is given. Although estimates of the ice properties are made from these data, there are not sufficient data to determine how reliable these estimates are.

Equations for the creep of a floating ice sheet are also given when the load increases linearly with time. A discussion is given of the singularities occurring in the solution when Reissner's plate theory is used rather than the thin-plate theory.

PREFACE

This report was prepared by Donald E. Nevel, Research Physical Scientist, of the Applied Research Branch, Experimental Engineering Division, U.S. Army Cold Regions Research and Engineering Laboratory.

This paper is written with the view of utilizing a mathematical theory to provide a solution needed by practical engineers. Sometimes engineers do not have sufficient time or theoretical background to apply highly mathematical theories to a particular problem. On the other hand, those who develop mathematical theories often do not have the inclination to apply these theories to particular problems and to extract from the results the information which an engineer wants. The approach taken in this paper attempts to bridge this gap.

The author would like to thank Carl Long for his guidance in preparing this thesis and Shunsuke Takagi for his discussion of some of the mathematical details in this paper. In general, appreciation is given to the staff members at CRREL for their support in pursuing the theoretical development of the entire bearing capacity problem of a floating ice sheet, and in particular, to Andrew Assur for his stimulating ideas and Guenther Frankenstein for his practical, down-to-earth approaches. A word of thanks should also be given to Kevin Carey who edited this manuscript and to Donna Gerow for the typing with all its tedious equations.

TABLE OF CONTENTS

LIST OF TABLES

LIST OF FIGURES

LIST OF SYMBOLS

A. Symbols for material constants

G is the shear modulus,

ν is Poisson's ratio,

E_1, E_2, and E_3 are elastic constants as defined in Figure 4a page 25,

E_o is the secondary creep elastic constant defined by $1/E_o=1/E_1+1/E_2$

η_1, η_2, and η_3 are viscous constants defined in Figure 4a page 25,

η_o is the viscous constant for secondary creep defined by $1/\eta_o=1/\eta_1+1/\eta_2$,

E is the dimensionless elastic constant for primary creep defined by $E=E_o/E_1$

τ is the dimensionless viscous constant for primary creep defined by $\tau = (\eta_o E_2)/(\eta_2 E_o)$

η is the dimensionless viscous constant for tertiary creep defined by $\eta = \eta_o/\eta_1$

ξ is the dimensionless elastic constant for tertiary creep defined by $\xi = (\eta_o E_3)/(\eta_3 E_3)$

B. Symbols for stress, strain, and deflection

ε is strain

σ is stress

w is vertical deflection

w^o is vertical deflection at time zero

w^* is $w-w^o$

σ_r is the radial stress

σ_r^o is the radial stress at time zero

σ_r^* is $\sigma_r-\sigma_r^o$

σ_θ is the tangential stress

σ_θ^o is the tangential stress at time zero

σ_θ^* is $\sigma_\theta-\sigma_\theta^o$

C. Symbols for time and horizontal distance

t is time

T is $E_o t/\eta_o$, dimensionless time

s is the Laplace transform variable of T

ℓ is the flexural rigidity length (see equation 13a, page 32)

a is the radius of the load distribution

A is a/ℓ, dimensionless radius of load distribution

r is radial coordinate

R is r/ℓ, dimensionless radial coordinate

β is the Hankel transform variable of R

D. Symbols for functions

See reference 64 for notations.

$H(x)$ is a unit step function

$\log(x)$ is the logarithmic function to the base e

$J_o(x)$ is a Bessel's function of order zero

$J_1(x)$ is a Bessel's function of order one

$\mathrm{kei}(x)$ is a Kelvin function

$\mathrm{ker}(x)$ is a Kelvin function

$\mathrm{bei}(x)$ is a Kelvin function

$\mathrm{ber}(x)$ is a Kelvin function

$E_1(x)$ is an exponential integral function

$E_i(x)$ is an exponential integral function for a negative argument

γ is Euler's constant

${}_1F_1(a,b,x)$ is a confluent hypergeometric function

E. Other symbols

∇_r^2 is the harmonic operator in polar coordinates

D is the flexural rigidity

D_T is the time operator part of the flexural rigidity

C is the correction factor if the ice properties are not uniform (see equation 40, page 38)

k is the unit weight of water

h is the ice thickness

z is the vertical distance measured from the neutral axis

q is the pressure applied from the load

P is the load

$\dot{P}$ is the load rate

Q is the vertical shear force per unit length

ψ^2 is $(2-\nu)h^2/[10(1-\nu)\ell^2]$, a factor which enters Reissner's plate theory

F. Special symbols

In general the Hankel transform of the solution contains terms of $e^{-\alpha_i T}$ where α_i depends upon the Hankel transform variable β and the material constants. The specific symbols for the various α_i's are:

α is defined for secondary creep by $1/(1+\beta^4)$

α_1 and α_2 are defined for primary creep in equation 76 page 59.

α_3 and α_4 are defined for tertiary creep in equation 96 page 66.

α_5 is defined for secondary creep using Reissner's plate theory in equation 119b page 88.

λ_1 is $\alpha_1(\beta=0)$

λ_2 is $\alpha_2(\beta=0)$

λ_3 is $\alpha_3(\beta=0)$

λ_4 is $\alpha_4(\beta=0)$

CREEP THEORY FOR A FLOATING ICE SHEET

by

Donald E. Nevel

INTRODUCTION

Floating ice sheets frequently have heavy loads imposed upon them. Vehicles use ice sheets as convenient bridges to cross rivers and lakes, and in some cases as convenient highways by following rivers. Generally these uses are by individuals or private enterprises, but recently the Saskatchewan Department of Highways has maintained a public road over an ice sheet between two towns that are on opposite sides of a lake. Military and civilian aircraft have for years used floating ice sheets as landing strips during the winter. For example, the U.S. Navy maintains a landing field on the sea ice at McMurdo, Antarctica. The C5-A aircraft, having a gross load of 767,000 pounds, has even been considered for landing at McMurdo.

More recently, oil companies have used floating ice sheets in the exploration for oil offshore in the Canadian Archipelago. This operation includes not only transportation across the ice, but also use of the floating ice as a drilling platform. A sustained load on the ice of 1 to 2 million pounds for a three to four month period is not uncommon at the sites of these exploratory holes. The Arctic Petroleum Operators Association has sponsored long-term bearing-capacity tests on sea ice over a range of ice thicknesses. Presently these results are still considered proprietory by APOA. In addition to these Canadian activities plans are being made for similar drilling operations off the north shore of Alaska.

Most of the world has recently recognized the critical situation faced by society with respect to energy supplies. As part of this situation, petroleum exploration, development, and distribution have received increased attention from both industry and the public. A significant share of this petroleum activity is focused in the arctic regions. In view of these energy-related activities in the Arctic, predicting the deflection and bearing capacity of floating ice sheets under sustained load becomes important for the economical, social, and political welfare of our country as well as the world as a whole.

Various types of bearing-capacity problems have been addressed in practical operations in the past. The most useful bearing-capacity problems are for very large floating ice sheets which have loads uniformly distributed over circular or rectangular areas. For analytical treatment, it is sometimes useful to assume that that the horizontal boundaries of the ice sheet extend to infinity. Other important problems are associated with cracks in the ice sheet. Natural cracks occur along shore lines due to water-level changes, and they also occur within the ice sheet itself due to pressures caused by wind, water, and thermal forces. Frequently, arctic sea ice separates along a crack, creating an open water area called a "lead." Crossing of these "leads" has resulted in a number of accidents due to the reduced bearing capacity near a free ice edge. Recently, Bell Telephone has used an ice sheet as a working platform for laying telephone cables across a lake. When the ice was cut to drop the cable through, a man-made separation, or lead, occurred. A similar operation is contemplated for laying gas and oil pipelines between the islands of the Canadian Archipelago.

Among other problems related to ice sheets are those of resonance and impact. Resonance problems can occur for vibratory loads and for loads moving with a constant velocity across the ice sheet. Impact type problems may be represented by the air dropping of equipment by parachute. Conversely, if a load remains for a long time on the ice sheet, the ice will creep. Observations show that a load which does not initially crack the ice sheet may crack it after some time and eventually break through under the influence of creep. Sometimes after sufficient deflection due to creep, water may seep through the cracks and flood the deflected portion of the ice sheet which helps the breakthrough process.

This paper confines itself to only one of the many problems raised by man's utilization of ice sheets, and that is creep, the long-term deformation of a floating ice sheet under a steady load. It is the purpose of this paper to develop a method for predicting the deflection and stress as a function of time for an ice sheet undergoing creep.

STATE-OF-THE-ART

First, a review of the state-of-the-art regarding bearing capacity of floating ice sheets will be given. This review includes references to efforts which have made improvements in the analytic methods of predicting the bearing capacity. The arrangement of the material is according to problems and the chronological development of their solutions. Other types of references on bearing capacity of floating ice sheets are contained in a paper by A.D. Kerr [1]. There are also many more references concerning the related problem of the bearing capacity of concrete pavements. In this case the soil is treated as an elastic foundation (which has become known as a Winkler or a Winkler-Zimmerman foundation). Hetényi [2], in a review article, has discussed the history and the nomenclature of these elastic foundation models.

In general the tensile strength of ice is lower than the compressive or shear strength. When an ice sheet is bent, it cracks along lines of maximum tensile stress. The failure criterion which is most frequently used is that the ice cracks when a limiting tensile stress is reached. This is the failure criterion which is considered in this paper.

Recently F.D. Haynes [3] and Langford and Francis [4] have shown that this maximum tensile stress depends upon the principal stresses. D.E. Nevel and F.D. Haynes [5] have attempted to interpret the meaning of this data.

The most frequently used bearing capacity problem is an infinite sheet of finite and constant thickness which is uniformly loaded over a circular area. The imprint that a pneumatic tire makes with the ice closely simulates this loading condition.

Heinrick Hertz [6] in 1884 was the first to consider this problem. He represented the ice sheet with the thin elastic plate theory in his mathematical model. The static water pressure on the bottom of the plate is proportional to the plate's deflection. For a concentrated load, he simply presented the solution for the deflection of the plate in the form of an integral. He recognized this integral as being the sum of two modified Bessel functions with complex arguments. Hertz expanded the Bessel functions into a series, and by differentiating the series, an expression for the stresses was obtained. He then integrated the series for the stress, keeping only the most significant term, to obtain the stress directly under the center of a load uniformly distributed over a circular area. Hertz recognized the fact that if the diameter of the load distribution approached zero, the stress approached infinity. He suggested that the smallest diameter that should be used in the formula be equal to the ice thickness. Note that Hertz only found the first term of the series for the stress directly under the load. He did not find the stress at an arbitrary point, nor did he find the general solution to the fourth-order differential equation.

August Föppl [7] in 1907 next considered the problem. He considered Hertz's method of Bessel functions as far too specialized and unfamiliar to most readers, so he developed the four general solutions of the differential equation by means of power series. These power series were either Bessel functions or linear combinations of Bessel functions. Föppl did not solve the infinite plate problem.

It was left to Ferdinand Schleicher [8] in 1926 to present the solution in a form that was usable for the engineer. He first showed how the fourth-order differential equation could be separated into two second-order equations which were recognized as Bessel's differential equations. He expressed the general solution of the equation as a linear combination of $-(2/\pi)$ kei(x), $-(2/\pi)$ ker(x), -bei(x), and ber(x). The Bessel functions bei(x) and ber(x) were introduced by Sir William Thompson (Lord Kelvin) in 1889, and Russell introduced kei(x) and ker(x) in 1909 according to Watson [9]. These four functions are sometimes referred to collectively as Kelvin functions. Schleicher tabulated his functions and their first derivatives. Formulas for the integrals and higher order derivatives were given in terms of the functions and their first derivatives. Schleicher developed the solution for the load uniformly distributed over a circular area by considering two regions of the plate. A solution for the plate under the load was connected to a solution for the plate outside the load by the proper boundary conditions. The constants of integration were determined from four simultaneous equations. He gave a formula for the deflection only, but the stress formulas could easily be developed by the reader. In his book, Schleicher also presented solutions for many other problems concerning axially symmetrical plates on an elastic foundation.

Max Wyman [10] contributed to the solution of the problem in 1950 by simplifying the constants of integration. He solved the concentrated load problem again. He then integrated this solution to obtain the case of the uniform circular load. In order to perform the integration, he developed what are known as "addition theorems" for the Kelvin functions. He developed the general equation for the stress and specifically applied it to the maximum tensile stress under the load for a floating ice sheet.

With the coming of the computers in the 1950's, the evaluation of these functions became easier. In general for practical application, a series expansion is sufficient since the deflection and stresses decay very rapidly at large distances. D. Nevel [11] gives an efficient method for calculating these functions and their first derivatives, if all the functions are needed. Nevel's method consists of using a recurrence formula between the functions rather than just for one function.

The problem of predicting an infinite stress for a concentrated load was first recognized by Hertz. The fundamental difficulty arises because of the approximations of the thin-plate theory. When any distance becomes small relative to the plate thickness, the assumptions on which the plate theory is based become invalid. This problem is expecially acute for bearing capacity of ice sheets, since the imprint diameter of a pneumatic tire may be much smaller than the thickness of the ice.

In 1926 H.M. Westergaard [12] presented a formula for the solution of this infinite-stress problem. His formula was based on the solution of a three-dimensional elastic layer which was developed by A. Nadai [13]. Nadai considered a finite, axially-symmetrical, elastic layer whose bottom surface was free of stresses and whose top surface had a normal load, uniformly distributed over a circular area. There were no vertical deflections on the circumferential surface; however, there were stresses and radial displacements acting on this surface. By superimposing a solution for pure bending, a solution was obtained that had no radial or tangential bending moments on the circumferential surface. By properly choosing the constants of integration, the vertical deflection at any given depth on the circumferential surface could be made to disappear. This solution corresponds to a simply-supported plate without an elastic foundation.

Westergaard numerically evaluated this solution for the maximum stress when the radius of the plate was five times the thickness of the plate. When the radius of the load was greater than 1.724 times the plate thickness, he found that the thin plate theory gave the same numerical answer as the three-dimensional theory. When the radius of the load was less than 1.724 times the plate thickness, he found a difference between the two theories. He then gave an equivalent load radius that if used in the thin plate theory, will predict the same maximum stress as the three-dimensional theory. Approximately the same results were obtained with layers whose radius-to-thickness-ratios were other than five. Westergaard then stated, "the results may be applied generally to slabs of proportions such as are found in concrete pavements, with any kind of support which is not concentrated within a small area close to the load." Although his results are in a very useful form, it isn't obvious that his generalized statement is true.

In 1933 S. Woinowsky-Krieger [14] developed the three-dimensional elastic layer solutions for plate problems both in rectangular and radial coordinates. He presented numerical results for the maximum tensile stresses in a simply-supported and a clamped-supported axial symmetric elastic layer without an elastic foundation. Woinowsky-Krieger also developed expressions for the deflection of plates on an elastic foundation but he did not discuss the stresses.

In 1970 D.E. Nevel [15] developed a formula for the maximum tensile stress in an elastic layer on an elastic foundation. Numerical results were obtained and compared with results obtained by using Westergaard's equivalent radius of load in the thin-plate theory. This comparison showed that the two results were numerically very close. Hence, for simplicity, Westergaard's method can be used for the stress on the bottom surface of the plate directly under the center of the load. For the state of stress near this point, Nevel's solution can be used. For the state of stress far from this point, the thin-plate theory as expressed by Wyman can be used.

Tracked vehicles, buildings, and storage areas present rectangular load imprints on the ice sheet. The solution of this category of problem is associated with the development of the solution for rectangular plates on an elastic foundation. The first such treatment was by H. Happel [16] in 1920, who assumed a solution in the form of a double series and obtained the coefficients of the series by the Ritz method.

Almost simultaneously, Lewe [17] and Westergaard [18] in 1923 published papers giving the solution for rectangular plates on an elastic foundation in the form of Fourier series. Lewe used Navier's [19] method of solution of a double Fourier series, while Westergaard used Levy's [20] method of a single Fourier series. Westergaard showed how a large variety of boundary conditions for rectangular plates on elastic foundations could be solved. In order to show the generality of his solution, consider the rectangular plate with supports along two opposite edges as shown in Figure 1. Westergaard stated that along these supported edges, three kinds of boundary conditions could be solved by Levy's method:

1) Both edges are simply supported; i.e., the deflection and the bending moment in the x-direction are zero along each boundary.

2) The slope in the x-direction, shearing forces, and twisting moments are zero along each boundary, which is the same boundary condition created by symmetry from loads of equal magnitude equally spaced along the x axis as shown in Figure 2.

3) The distance between the two supports goes to infinity; i.e., the deflection and the slope in the x-direction are zero as x goes to infinity. In this case the Fourier series goes into a Fourier integral.

These three boundary conditions occur because of the nature of the

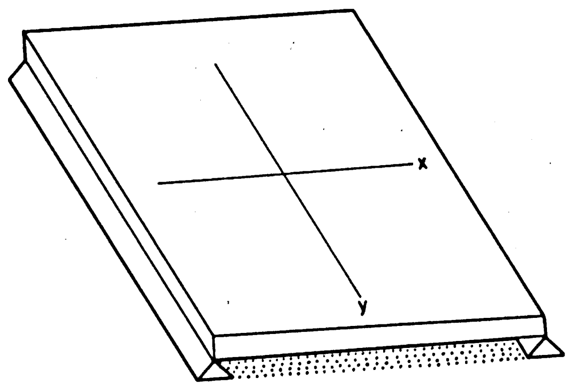

Figure 1. Rectangular plate on an elastic foundation.

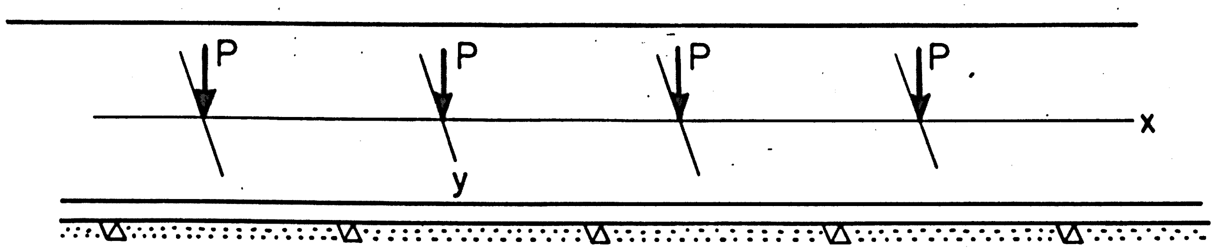

Figure 2. Boundary conditions due to symmetrical loads

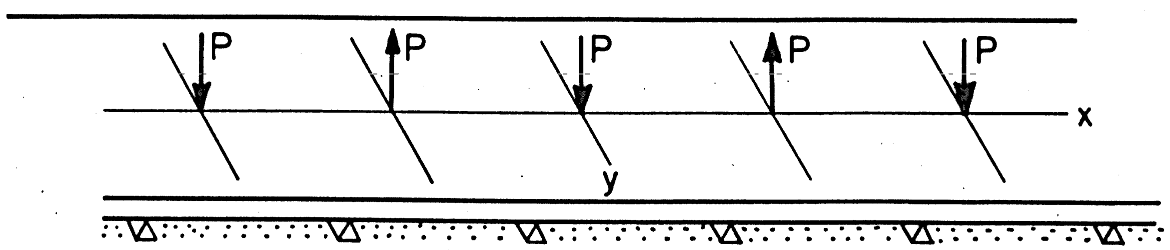

Figure 3. Boundary conditions due to anti-symmetrical loads.

Fourier series which was taken in the x direction. On each of the other two boundaries, which are perpendicular to the y-axis, any boundary condition from thin-plate theory can be specified. In addition, either one or both of these boundaries may be located at infinity.

In 1953 R.K. Livesley [21] pointed out that a simply-supported boundary condition is obtained along a line equidistant from two loads of equal magnitude, but acting in opposite directions. This anti-symmetrical loading was further elaborated on by A.D. Kerr [22]. Hence the set of simply-supported boundary conditions by Westergaard can be obtained from loads of the same magnitude, but of alternating directions, equally-spaced along the x-axis as shown in Figure 3.

Westergaard solved the problem of a plate on an elastic foundation that extends to infinity in all horizontal directions, i.e. the cases of Figure 2 and 3. He also let the distance between loads go to infinity to obtain the concentrated-load solution in rectangular coordinates. He did not consider loads uniformly distributed over a rectangular area, but the integration from the concentrated load is straightforward since it involves integrating an exponential multiplied by sines and cosines.

Hence, Westergaard had solved or given the method for solution in rectangular coordinates for the principal problems associated with floating ice sheets as early as 1923. The most important of these problems is the rectangular load on an infinite sheet. For this case the solution is in the form of a Fourier integral which is non-integrable. For ease of numerical computation, the author recommends the series solution corresponding to Figures 2 or 3, with the distance between loads sufficiently large so that there is no interaction between the loads. It turns out that the Fourier cosine series representation for Figure 3 is summed over odd integers only, while the one for Figure 2 is summed over both odd and even integers. Hence, it is easier for numerical computation to use the solution obtained from Figure 3. This procedure greatly simplifies the numerical calculation, but appears not to have been recognized before.

The other important boundary conditions for floating ice sheets are associated with cracks. At the shoreline, there is usually a crack caused by flexing of the ice sheet due to small changes in water level. The conditions along this crack are zero bending moment and zero deflection. This corresponds to a simple support, and can be represented with two anti-symmetrical loads on an infinite sheet. Thus, this case is solved by the superposition of two solutions.

If a crack occurs in the ice sheet other than at the shore, the solution is more complicated. For a crack that does not open, the deflections are equal on both sides of the crack, but the bending moment is zero across the crack. Using Westergaard's method, M.S. Skarlatos [23] in 1949 has solved this type of problem. This solution has not been utilized frequently for floating ice sheets, because the more critical case occurs when the ice separates and the crack opens.

If the crack in the ice sheet separates, a free-edge boundary condition occurs. Westergaard also solved the problem of a concentrated load at or near a free edge in 1923. In 1943, G.S. Shapiro [24] integrated the concentrated load to obtain line loads in either the x- or y- direction for this semi-infinite plate. In 1965 Nevel [25] integrated to obtain a load uniformly distributed over a rectangular area for the same problem. In this case as before, numerical computation is facilitated if the solution is obtained from a row of anti-symmetrical loads widely spaced, since this provides a solution in series rather than integral form.

Other boundary conditions are solvable for rectangular plates other than the ones shown by Westergaard. H.J. Fletcher and C.J. Thorne [26] generalized the simply-supported set of boundary conditions of Westergaard. They solved the same problem when the deflection and bending moments are given as functions of y along each support.

The previously discussed treatments have considered the maximum stress produced in a floating ice sheet. An analysis of this type will predict the first crack that occurs under a load. Experimental observations have shown that the load does not fall through the ice sheet upon initiation of the first crack. In other words, practical failure does not occur with the first crack. First-crack analysis produces a safe bearing capacity for operations in which one does not want the load to fall through the ice. There are times, however, in which one needs to operate on the ice sheet with less margin of safety under emergency conditions. On the other hand, there are times in which the object of the loading is to break through the ice sheet.

Let us consider the case of safe emergency operations first. If a uniform load, distributed over a circular area, is of sufficient magnitude to produce a crack in the ice, the crack will propagate from the load in a radial direction. This seems reasonable since Wyman's solution predicts that the tangential stresses are greater than the radial stresses near the load. Of course, directly under the load they are equal. The next crack would tend to occur at 90° to the first crack, forming four 90° wedges. (Sometimes the second crack is not at 90° because the ice sheet is not uniform in its properties.) Then the next set of cracks divides the four 90° wedges in half, producing eight wedges. In all cases, the radial cracks that form the wedges propagate radially outward and stop some distance from the load. If the properties of the ice are not uniform, wedges of angles other than 45° may occur. In any case the wedges always try to divide themselves in half unless the non-uniform ice properties cause the crack to occur elsewhere. The total number of wedges that have been observed are from five to eight. Commonly six wedges are formed. Sometimes these radial cracks, which are caused by tension on the bottom of the ice sheet, are difficult to see because of snow on the surface, or because they have not propagated through to the top of the ice. After radial cracking, the next crack to occur is circumferential. That is, the wedges break off. Andrew Assur has suggested that the prediction of this circumferential crack, by analysis of a wedge, may be a good criterion for emergency operation.

In a series of papers, D.E. Nevel [27,28,29] developed the solution of an infinite wedge on an elastic foundation. The wedge was considered a beam of variable width whose sides were free of stress. This stress-free condition may not be entirely valid if two adjacent wedges interact under non-symmetrical loading.

In 1960 D.F. Panfilov [30] published experimental results for the final break-through of loads on thin ice sheets. In a paper published in 1972, D.E. Nevel [31] showed the close agreement between the results predicted from the wedge theory as compared to Panfilov's experimental data. Hence it appears that the wedge theory can be used to predict bearing capacities for emergency operations. The one difficulty remaining in this area is the problem associated with two or more loads near each other. For predicting the first radial crack, the stresses could simply be added by superposition. However, the two or more adjacent loads will produce different radial crack patterns, and hence superposition of the stresses is not justified for the later stages of crack formation.

From laboratory tests by the author, the first circumferential crack to occur in a thin ice sheet under load does not always produce final break-through. In these instances, a second crack which breaks the wedge at a farther distance from the load often produces the final breakthrough.

Experimental field tests by Guenther Frankenstein [32] have shown that for thick ice sheets, the first circumferential crack does not produce final breakthrough. In this case, additional cracking of the wedge occurs parallel to the first circumferential crack, but closer to the load. Final breakthrough occurs by these circumferential bending cracks close to the load. This circumferential crack progression for thick ice is probably caused by wedge interaction. For emergency operations with either thin ice or thick ice, one usually would not want to operate with a load greater than that which would produce the first predicted circumferential crack.

Let us now consider the case of loading the ice sheet with the object of ensuring breakthough. This type of loading can occur when submarines need to surface through the ice, or when air-cushion vehicles are used for ice-breaking operations. For this type of analysis, the ice is assumed to be perfectly plastic.

Anders Johannson [33] in 1947 was the first to apply a perfectly plastic theory to the problem of a plate on an elastic foundation. He used a square yield criterion. Later, in 1960 G. Meyerhof [34] solved a number of problems for the perfectly plastic plate on an elastic foundation with the condition that the material of the plate obeyed a

Tresca yield criterion. In 1972 Max D. Coon and M.M. Mohaghegh [35] considered the same analysis for an infinite plate on an elastic foundation when the plate obeyed either a square, Tresca, or Coulomb yield criterion. Of these three criteria, the Tresca criterion produces the smallest allowable bearing capacity load. All of Coon and Mohaghegh's results predict loads higher than Panfilov's breakthrough loads, as might be expected from a limit analysis.

So far we have considered static loads only. The most important dynamic problems are a load moving with uniform velocity, a vibrating load, and an impact load. In 1950 D.T. Holl [36] developed a general dynamical solution for a plate on an elastic foundation. The vertical acceleration of the plate was considered, but no acceleration of the elastic foundation was included. In 1953 R.K. Livesley [21] solved the problem of a load that is uniformly distributed over a rectangular area, and is moving with a constant velocity across a thin plate resting on a static, elastic foundation. Livesley incorrectly analyzed the singularity of his integral solution and obtained incorrect critical velocities at which the solution diverges. (In general, a "critical velocity" is one which makes the solution become infinite or maximum.)

In an attempt to include the dynamics of the water in the moving-load problem, J.T. Wilson [37,38] in 1955 joined together two previously solved problems. He utilized Greenhill's [39] solution for the response of a floating plate to a water wave propagating in one direction, and Hertz's [6] solution for a static concentrated load. Wilson chose the wavelength of the waterwave equal to the diameter of the smallest circle which is the locus of points having zero deflection in the plate. Although this coupling procedure is incorrect, it did predict critical velocities which were only 5% too high for deep water. For shallow water the predicted velocities are as much as 33% too high.

For the first time, D.E. Kheisin [40,41] in 1963 solved the moving-load problem in a way which included the dynamics of the water. The water was considered to be an incompressible, inviscous fluid and the velocity-squared term in Bernoulli's equation was neglected. He incorrectly analyzed the singularities of his integral solution and arrived at the erroneous conclusion that the deflection under the load is finite at the critical velocity. No attempt was made to obtain values for these critical velocities.

In 1970, D.E. Nevel [42] solved the same problem again. By interpreting the singularities correctly, he arrived at a critical velocity which predicts infinite deflections and stresses. Numerical values for the critical velocity were given, and these values compare favorably with the limited experimental data that are available.

The case of a vibrating load acting on a plate resting on a static, elastic foundation was considered by D.T. Holl [36] in 1950. And then in 1962, D.E. Kheisin [43] first formulated this problem with the dynamics of the water included. Kheisin solved the problem for a concentrated load in 1967 [41]. In 1970 D.E. Nevel [44] solved the vibrating-load problem for a load uniformly distributed over a circular area, and he obtained numerical values. Nevel found that the applied frequency which caused a maximum stress was less than 0.2 cycles per second, and that at this frequency, the stresses were amplified only 5 to 10% compared to the static case. The applied frequency needed to obtain the maximum deflection is less than that for the stresses. However, the deflections can be amplified as much as 30%.

In 1967 D.E. Kheisin [41] solved the floating ice sheet problem under the influence of an impulse load, i.e. a load that is suddenly applied and removed. However, Kheisin did not consider the impact, or suddenly applied, load.

In 1968 Herbert Reismann and Yu-Chung Lee [45] considered the impact load, but they did not include the dynamics of the water foundation. In Reismann's formulation of the impact problem, plate theory was utilized. It has been the experience of the writer that failure of an ice sheet under impact loads occurs by punching through, rather than by bending. Hence, a plate-theory solution appears to be the wrong mathematical formulation. The three-dimensional elastic layer model would be a better representation. For the axially-symmetric elastic layer, the writer has solved the dynamic impact problem, but the solution is rather complex and is expressed in the form of a double integral. One integral is an inverse Hankel transform, while the other integral is an inverse Laplace transform. Since no numerical results were obtained the solution was never published.

With the foregoing material as background, it is now possible to consider the problem of creep of a floating ice sheet under loads of long duration. ~~This is the main theme of this paper.~~

D.E. Kheisin in 1964 [46] was the first to consider the floating ice sheet problem using linear viscoelastic theory. He considered the ice to be incompressible under hydrostatic stress, and the shear modulus to be represented by a Maxwell model which is shown later in Figure 7a. He applied Fourier transforms with respect to the Cartesian space coordinates x and y in order to reduce the partial differential equation of the plate to a first order differential equation in time, which was easily solved. Kheisin converted the transformed space variables to polar coordinates, and integrated with respect to the angle, leaving his solution in the form of a single integral. The double Fourier transform method which he applied is equivalent to a Hankel transform. In his analysis Kheisin considered a concentrated load that is applied either suddenly or linearly with time. For the deflections under the load he expanded the integrand into a series about time equal to zero, and then integrated term by term to obtain a solution valid for short time. He did not discuss the stresses in the ice sheet.

In 1966, D.E. Nevel [47] solved the same problem as Kheisin, but Nevel considered a distributed load. Nevel used E.H. Lee's correspondance principle, which left the solution in the form of an inverse Laplace transform, a complex integral. For the point directly under the load, he expanded the integrand into a series about zero with respect to the radius of the load distribution, and then integrated the first two terms. Numerical values were determined for the deflections and bending moments when the load is applied either suddenly or linearly with time. For short time, the solution reduces to that of Kheisin. Nevel also considered the solution for a viscous model in order to show how the two models approach each other for large time.

In 1967, William L. Ko in a work by Garbaccio [48] also considered a distributed load on a viscoelastic floating ice sheet. He assumed Poisson's ratio constant, and Young's modulus to be represented by the model shown later in Figure 6a. Ko used Reissner's plate theory, which includes the deformation due to vertical shear forces. He used a Hankel transform with respect to the radial distance, and a Laplace transform with respect to time. Taking the inverse Laplace transform, the solution was left in the form of an inverse Hankel transform. Ko's solution is easier to evaluate numerically than Nevel's because the integral is real rather than complex.

Garbaccio [49] numerically evaluated Ko's solution for specific values (Poisson's ratio = .3, E_1 = 71,000 psi, E_2 = 85,000 psi, η_o/E_1 = 14 min, and η_2/E_2 = 9 min) rather than for non-dimensional parameters which occur in Ko's solutions. In addition, Garbaccio's numerical answers show that the deflection is due primarily to vertical shear forces rather than due to bending moments. However this has not been observed, and thus it is reasonable to suspect that there is an error in his numerical evaluation.

Using methods similar to Kheisin, IAkunin [50,51] has solved the same problem as Ko except that IAkunin used thin-plate theory rather than Reissner's plate theory. He has compared his results to floating ice sheet tests and obtained average values of E_2/E_1 = .2 and η_2/η_o= .05. Unfortunately, only an abstract of IAkunin's work is available to the Western literature.

It should be pointed out that Ko [48] was not the first to solve the problem of a plate on an elastic foundation using Reissner's plate theory. The elastic axially symmetric plate on an elastic foundation was considered by Naghdi and Rowley [52] in 1953 and by Daniel Frederick [53] in 1956. Frederick [54] also treated the problem in rectangular coordinates in 1955. However, the method of these authors differs from that of Ko's (this difference is discussed later in this paper). Furthermore, it should be stated that Reissner's theory has not yet produced results significantly different than those of the thin-plate theory when applied to bearing capacity of ice sheets.

M.G. Katona [55] in 1974 and K.D. Vaudrey and Katona [56] in 1975 developed a finite element computer program for a floating ice sheet. Their program assumes a linear viscoelastic stress-strain relation and is limited to axially symmetric loads. They assumed that Poisson's ratio is constant and that Young's modulus is represented by a spring in series with a number of delayed elasticity elements. They stated that usually two delayed elasticity elements are sufficient to represent the creep properties of most materials. The material constants are permitted to depend on the vertical position in the ice sheet.

In 1975 K. Hutter [57] developed a general nonlinear plate theory for floating ice, with constitutive equations based upon a thermorheologically simple material. These constitutive equations are linear, but the material constants depend upon temperature. For an ice sheet, the temperature is a function of the depth in the ice sheet and time. Although a very generalized theory is presented, Hutter's theory was not utilized to solve any problems.

APPROACH

The objective of this paper is to develop a theory that will predict the deflections and stresses in a floating ice sheet which sustains a load over an extended length of time. This means that the constitutive equations must be sufficiently general to include all the observed creep properties of ice. On the other hand, the constitutive equations must be formulated in a manner that permits relevant problems to be solved. A comparison of a particular solution with actual observations will then determine how applicable the theory is. Unfortunately, very few creep tests on floating ice sheets have been conducted, and for those that have been conducted, most of the data are unavailable. A discussion is given in this paper about the available data, but final determination of the applicability of this theory will have to wait until better data are obtained.

Most of the information that we know about the constitutive equations for ice under creep has been determined from uniaxial tension and compression tests. A literature survey of these and other results can be found in other references such as Kuo [58] and Sumskij [60], and will not be repeated here. However, a brief description of creep of ice will be given in order to justify the representation of the constitutive equations.

A typical creep curve for polycrystalline ice under a constant uniaxial stress is shown in Figure 4b. This curve displays an instantaneous elasticity, a delayed elasticity, a steady creep, and finally an accelerating creep that becomes large as time increases. These types of creep curves have shown that it takes a longer time to reach the steady state creep under low stress than it does under a higher stress. Sometimes for low stress the accelerating creep is never reached within the test time. For extremely high stress, the delayed elasticity occurs very rapidly. Obviously the temperature of the ice affects these results also. A warmer temperature permits the ice to flow more easily.

Glaciologists have generally only reported in the literature on the steady part of the creep curve. They have investigated the minimum creep rate as a function of temperature and stress level. They have found that the minimum creep rate is proportional to σ^n where σ is the applied stress and n is an experimental number. For high stresses n is in the range for 2 to 4. For low stress levels it is about 1.

One would like to know if the stress-strain equation is linear with time held constant. Since the minimum creep rate occurs at different times, most of the data reported by the glaciologists are difficult to interpret. However, some data have been reported from which useful information can be obtained.

From direct-tension creep tests below 2 kgf/cm^2 on snow-ice at -5°C for up to 5 hours duration, Jellinek and Brill [59] have shown a linear stress-strain relation for constant time. Kuo [58] has reported on compressive stress creep tests on snow ice at -4.5°C that extend considerably into tertiary creep. From his data one can conclude that the stress is nonlinear with strain for constant time when the stress is greater than 7 kgf/cm^2. Although other creep tests have been conducted, the data have not been reported in a manner that can help establish the limit of linearity under constant time.

The maximum stresses that will occur in a floating ice sheet under safe loading will be 7 kgf/cm^2 or less, and these will only occur locally near the applied load. Most of the ice sheet will experience a much lower stress level. Therefore, it seems reasonable to use a linear stress-strain relation to analyze the floating ice sheet problem. Not only is it easier to solve linear problems, but the superposition principle can be used for more than one load.

In this paper the stress-strain relation for ice will be represented by the six element linear viscoelastic model as shown in Figure 4a. Each of these elements is either a spring or a dash pot with the symbols E_1, E_2, E_3, η_1, η_2, and η_3 signifying positive quantities. If a stress σ is applied to this model at time zero, the resulting strain ε will be

$$\varepsilon = \sigma \, [1/E_1 + t/\eta_1 + (1-e^{-E_2 t/\eta_2})/E_2 + (e^{E_3 t/\eta_3}-1)/E_3] \qquad (1)$$

where t is the time. This equation is shown in Figure 4b and it exhibits all the features of a creep test on ice.

The E_1 element of the model provides instantaneous elasticity and is represented by the first term of equation 1. The η_1 element provides steady creep and is represented by the second term of equation 1. The E_1 and η_1 elements together are sometimes called a Maxwell model. The E_2 and η_2 elements provide delayed elasticity and are represented by the third term of equation 1. This delayed elasticity term is shown in Figure 5a. For large time it reduces to $1/E_2$. The E_2 and η_2 elements are sometimes called a Voigt model. The $-E_3$ and η_3 elements provide accelerating creep and are represented by the last term of equation 1. This accelerating creep term is shown in Figure 5b. For short time it reduces to t/η_3.

The time period before steady creep is commonly called primary creep. The steady creep period is called secondary creep. The time period beyond steady creep is called tertiary creep. The six element model of Figure 4a may be simplified depending on the time period of interest.

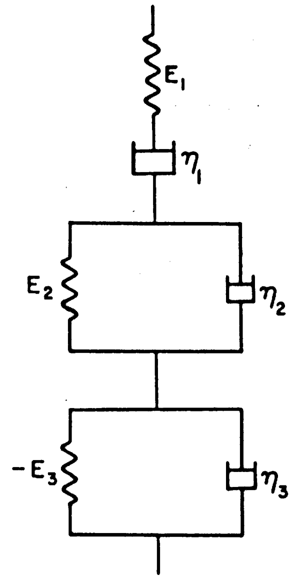

Figure 4a. Ice creep model

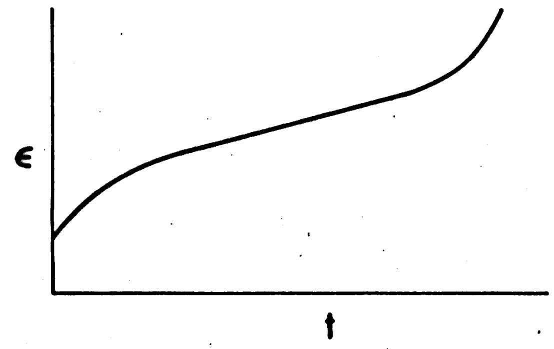

Figure 4b. Ice creep curve.

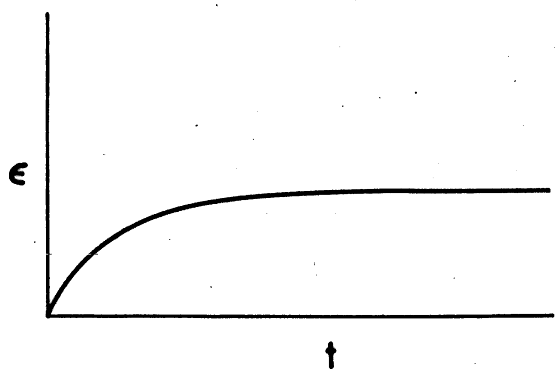

Figure 5a. A delayed elasticity element creep curve.

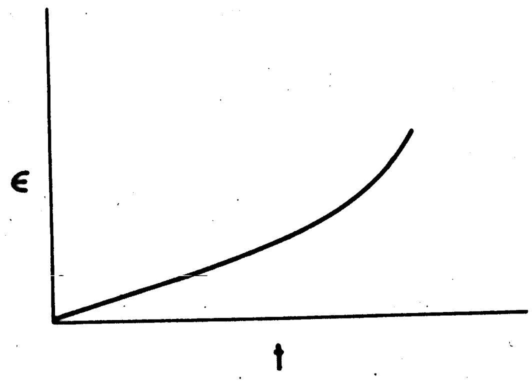

Figure 5b. An accelerating element creep curve.

In the primary creep range, the tertiary creep element reduces to t/η_3. Combining this with the steady state creep term, equation 1 becomes

$$\varepsilon = \sigma \, [1/E_1 + t/\eta_o + (1 - e^{-E_2 t/\eta_2})/E_2] \tag{2}$$

where $1/\eta_o = 1/\eta_1 + 1/\eta_3$. The corresponding model is shown in Figure 6a and the creep curve in Figure 6b.

In the secondary creep range the delayed elasticity has occurred as well as the previous reduction for the tertiary creep model. By combining elasticity elements, equation 2 becomes

$$\varepsilon = \sigma \, [1/E_o + t/\eta_o] \tag{3}$$

where $1/E_o = 1/E_1 + 1/E_2$. The corresponding model is shown in Figure 7a and the creep curve in Figure 7b.

In the tertiary creep range, the delayed elasticity has occurred, but the tertiary creep element cannot be reduced. Hence, equation 1 becomes

$$\varepsilon = \sigma \, [1/E_o + t/\eta_1 + (e^{E_3 t/\eta_3} - 1)/E_3]. \tag{4}$$

The corresponding model is shown in Figure 8a and the creep curve in Figure 8b.

Additional delayed elasticity elements and tertiary creep elements may be added to the six element model to obtain a better fit to the data. In fact, one may consider an infinite number of these elements. In this case a continuous spectrum is obtained rather than a discrete one and the material constants are represented by a creep function. If

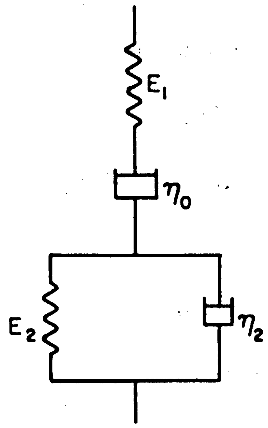

Figure 6a. Primary creep model.

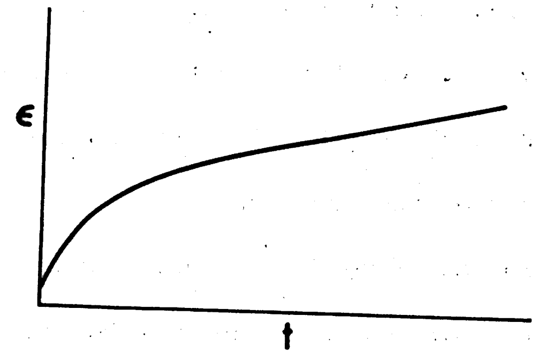

Figure 6b. Primary creep curve.

Figure 7a. Secondary creep model.

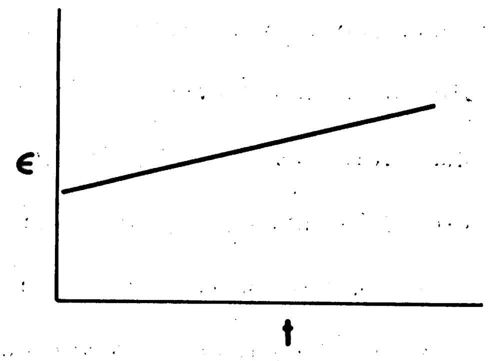

Figure 7b. Secondary creep curve.

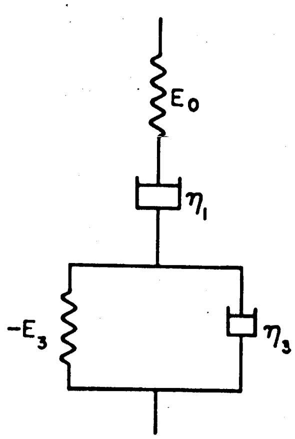

Figure 8a. Tertiary creep model.

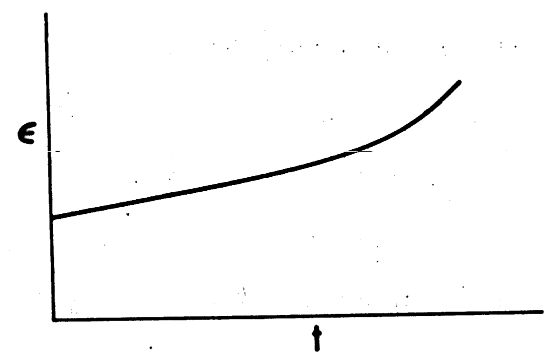

Figure 8b. Tertiary creep curve.

this creep function were known for ice, this would obviously be the best way to proceed. But with the uncertainty about the creep function it is better to choose the simplest possible model that will represent all the features of the creep curve for ice.

In fact from a practical point of view, the three models reduced from the six element model may be all that is necessary. For example, if one is interested in primary creep as it approaches secondary creep, the model of Figure 6 may be adequate with the right choice of material constants. The same model with a different set of material constants may represent the very beginning of primary creep. But it is probably unrealistic to expect a single primary creep element to be representative through the entire period of primary creep. With the single tertiary creep model of Figure 8, we can represent the onset of tertiary creep, but probably not follow it very far into tertiary creep. This concept of fitting simplified models to various regions of time is an important one which has not been fully appreciated before. For instance IAkunin [51] states that the model of Figure 7 is representative of ice for very short times, and that for longer times, the model of Figure 6 must be used. He obviously had the spring in Figure 7 equal to E_1, the same as the one in Figure 6. Hence, he matched the two models at time zero rather than at time infinity.

The concept of the tertiary creep element composed of $-E_3$ and η_3 is new and its implication in the physical creep process requires further investigation. The author was motivated to develop a simple method of representing tertiary creep after reading S. Kuo's work. Kuo represented tertiary creep with $\log\ [(1+ce^{-mt})/(1+c)]$ where c and m are constants. Although this expression may fit his data well, it becomes unmanageable if an attempt is made to solve a boundary value problem such as a floating ice sheet. The approach taken by the author is that the negative spring constant produces an accelerating creep curve similar to that observed for ice. Since the mathematical methods are similar for positive or negative spring constants, this approach allows a wide variety of boundary value problems which include tertiary creep to be solved within the framework of linear viscoelasticity. However, the negative spring constant should not be interpreted as a means of gaining an insight into the physical phenomenon, but rather as a convenient mathematical representation. Tertiary creep probably reflects the result of deteriorating property changes caused by the creep process. Possible explanations are recrystallization or intergranular deterioration phenomena. A resolution of this question requires further work and offers an intriguing challenge for the material scientist.

Using thin-plate theory to represent the ice sheet, the differential equation describing the deflections w of an ice sheet floating on the water is

$$D \nabla_r^2 \nabla_r^2 w + k w = q , \tag{5}$$

where

$$\nabla_r^2 = \frac{\partial^2}{\partial r^2} + \frac{1}{r}\frac{\partial}{\partial r} ,$$

and r is the radial coordinate,
w is the deflection of the ice,
k is the unit weight of water,
q is the applied pressure, and
D is the flexural rigidity.

The flexural rigidity D is assumed independent of r, and is defined by

$$D = \int \frac{2G\, z^2}{1-\nu}\, dz , \tag{6}$$

where z is the vertical distance measured from the neutral axis, G is the shear modulus, ν is Poisson's ratio, and the integration is performed over the thickness of the ice sheet. The shear modulus may be a function of z, but Poisson's ratio must be independent of z in order to define a neutral axis for the thin-plate theory. The flexural rigidity is usually defined with Young's modulus rather than the shear modulus. Young's modulus is equal to $2G(1+\nu)$.

The applied pressure q is assumed to be uniformly distributed within a circular area of radius r = a and is suddenly applied at time zero. The equation for q is

$$q = \frac{P}{\pi a^2} H(a-r)\, H(t) , \tag{7}$$

where P is the total load and H is a unit step function. $H(x)$ is 0 if x is negative and is 1 if x is positive.

We now consider ν to be a constant with respect to time, and 2G equivalent to the response of the six element model of Figure 4. Hence, we should replace 2G with the following differential operator

$$\frac{1}{2G} = \frac{1}{E_1} + \frac{1}{\eta_1 \partial/\partial t} + \frac{1}{E_2+\eta_2\partial/\partial t} + \frac{1}{-E_3+\eta_3\partial/\partial t} . \tag{8}$$

For the secondary creep model of Figure 7, equation 8 reduces to

$$\frac{1}{2G} = \frac{1}{E_o} + \frac{1}{\eta_o \partial/\partial t} . \tag{9}$$

Equation 9 is easily verified by adding the strains for each model in Figure 7. We can express the time t in a dimensionless manner by letting $T=E_o t/\eta_o$. Then equation 9 becomes

$$\frac{1}{2G} = \frac{1}{E_o} \left(1 + \frac{1}{\partial/\partial T}\right) . \tag{10}$$

We now define D_T by

$$2G = E_o\, D_T , \tag{11a}$$

and from equation 10

$$D_T = \frac{\partial/\partial T}{1+\partial/\partial T} . \tag{11b}$$

The reason for introducing equations 11 is to separate the elastic factor E_o from the time dependent operator D_T.

The material constants may be a function of temperature but we will assume the temperature to be constant in time. The temperature in the ice sheet is a function of the vertical distance z. However, we assume that the material constants E_o and η_o have the same temperature influence factor such that the ratio η_o/E_o is independent of temperature, and hence, independent of z. This concept of the ratio being independent of z is important, because it means that the E_o factor of equation 11a contains the z-dependent part, while D_T is independent of z. This concept is new and presented here for the first time.

We now consider the ratio D/k, and by substituting equation 11a into equation 6 we obtain

$$\frac{D}{k} = \frac{D_T}{k} \int \frac{E_o \, z^2}{1-\nu} \, dz \ , \tag{12}$$

where the time operator D_T has been taken outside the integral because it is independent of z. We now define ℓ^4 by

$$\ell^4 = \frac{1}{k} \int \frac{E_o \, z^2}{1-\nu} \, dz \ , \tag{13a}$$

such that equation 12 now becomes

$$\frac{D}{k} = D_T \quad \ell^4 \ . \tag{13b}$$

The symbol ℓ^4 has units of length to the fourth power. Hence, we will call ℓ the flexural rigidity length.

Let us now consider the differential equation 5. Dividing by k and substituting equation 13b we obtain

$$D_T \ell^4 \nabla_r^2 \nabla_r^2 w + w = q/k . \quad (14)$$

We now will make the distances "r" and "a" dimensionless by introducing $R=r/\ell$ and $A=a/\ell$. Then equation 14 with q from equation 7 substituted becomes

$$D_T \nabla_R^2 \nabla_R^2 w + w = \frac{P}{\pi k \ell^2 A^2} H(A-R) \quad H(T) . \quad (15)$$

In order to solve equation 15 we must substitute the operator D_T from equation 11b and multiply by $1+\partial/\partial T$ such that the time operator $\partial/\partial T$ does not occur in the denominator. Hence we obtain

$$[\frac{\partial}{\partial T}] \nabla_R^2 \nabla_R^2 w + [1 + \frac{\partial}{\partial T}] \quad w = \frac{PH(A-R)}{\pi k \ell^2 A^2} \quad [1 + \frac{\partial}{\partial T}] H(T) . \quad (16)$$

We will now solve the time part of equation 16 by means of a two-sided Laplace transform [61]. A two-sided Laplace transform of the deflection w is defined as

$$\bar{w}(s) = \int_{-\infty}^{\infty} w(T) \ e^{-sT} \, dT . \quad (17)$$

A two-sided Laplace transform is a Laplace transform that is integrated from $-\infty$ to ∞ rather than from 0 to ∞. The advantages of the two-sided transform is that the boundary conditions at time zero do not appear when integrating by parts. However, the transform of a function must be convergent at both $T = -\infty$ and $T=\infty$. In our case, H(T) provides the convergence at $T = -\infty$. Although there is a formula to obtain the inverse Laplace transform we do not explicitly need it in this paper. There are three properties of this tranform which we do need. The first is

$$\overline{\frac{\partial w}{\partial T}} = s\,\overline{w}\,, \tag{18a}$$

which is obtained from equation 17 by integrating by parts. The second two are

$$\overline{H(T)e^{-\alpha T}} = \frac{1}{s+\alpha}\,, \tag{18b}$$

and

$$\overline{H(T)T} = 1/s^2\,, \tag{18c}$$

which are obtained by integrating equation 17. Equations 18b and 18c can also be used to obtain the inverse Laplace transform of $1/(s+\alpha)$ and $1/s^2$.

Multiplying equation 16 by e^{-sT} and integrating with respect to T from $-\infty$ to $+\infty$ is called taking the Laplace transform of the entire equation rather than just a function. Doing this, and by using equations 18 with α=o, we obtain

$$[s]\,\nabla_R^2\,\nabla_R^2\;\overline{w} + [1+s]\,\overline{w} = \frac{PH(A-R)}{\pi k\ell^2 A^2}\;[1+s]\,\frac{1}{s}\,. \tag{19}$$

Dividing by (1+s) we get

$$\overline{D_T}\;\nabla_R^2\,\nabla_R^2\;\overline{w} + \overline{w} = \frac{PH(A-R)}{\pi k\ell^2 A^2}\;\frac{1}{s}\,, \tag{20}$$

where

$$\overline{D_T} = s/(1+s)\,. \tag{21}$$

If we compare equation 20 with equation 15 we discover that w and H(T) have been transformed, and the operator $D_T = (\partial/\partial T)/(1+\partial/\partial T)$ has become $\overline{D_T} = s/(1+s)$. That is, $\partial/\partial T$ has been replaced by s. This observation will prove useful when handling primary and tertiary creep later. We will now solve the spacial part of equation 20 by means of a Hankel transform [62]. A Hankel transform of the deflection w is defined as

$$\tilde{w}(\beta) = \int_0^\infty w(R)\, J_0(\beta R)\, R\, dR \,, \tag{22a}$$

and the inverse is defined by

$$w\,(R) = \int_0^\infty \tilde{w}(\beta)\, J_0(\beta R)\, \beta d\beta \,. \tag{22b}$$

A Hankel transform is nothing more than a double Fourier transform in the x,y coordinate system that has axial symmetry. Changing the x,y coordinates to r,θ and performing the integration with respect to θ we arrive at the Hankel transform. The one property of this transform which we will use is

$$\widetilde{\nabla_R^2 w} = -\beta^2 \tilde{w} \,. \tag{23}$$

This can be shown from equation 22a by integrating by parts.

Taking the Hankel transform of equation 20 by multiplying by $J_0(\beta R)$ R and integrating over R we obtain

$$\overline{D_T}\, \beta^4 \,\tilde{\bar{w}} + \tilde{\bar{w}} = \frac{P}{\pi k \ell^2 A^2}\, \frac{1}{s} \int_0^A J_0(\beta R) R dR \,. \tag{24}$$

By using the formula

$$\int J_0(z)\, zdz = z\, J_1(z) \,, \tag{25}$$

the integral in equation 24 can be integrated, and solving for $\tilde{\bar{w}}$ we get

$$\tilde{\bar{w}} = \frac{P}{2\pi k \ell^2} \frac{J_1(\beta A)}{\beta A/2} \frac{1}{s(1+\bar{D}_T \beta^4)} . \tag{26}$$

Taking the inverse Hankel transform of equation 26 we obtain

$$\bar{w} = \frac{P}{2\pi k \ell^2} \int_0^\infty \frac{J_1(\beta A)}{\beta A/2} \left[\frac{1}{s(1+\bar{D}_T \beta^4)}\right] J_o(\beta R)\beta d\beta . \tag{27}$$

In order to take the inverse Laplace transform of equation 27 we substitute $\bar{D}_T = s/(1+s)$ into the s factor of the integrand and obtain

$$\frac{1}{s(1+\bar{D}_T \beta^4)} = \frac{\alpha(1+s)}{s(s+\alpha)} , \tag{28}$$

where

$$\alpha = \frac{1}{1+\beta^4} . \tag{29}$$

The significance of α is that it is the negative root of a factor in the denominator. Applying partial fractions we get

$$\frac{1}{s(1+\bar{D}_T \beta^4)} = \frac{1}{s} + \frac{\alpha - 1}{s+\alpha} . \tag{30}$$

By substituting equation 30 into equation 27 and using equation 18b, the inverse transform is easily obtained, and equation 27 becomes

$$\frac{wk\ell^2}{P} = \frac{H(T)}{2\pi} \int_0^\infty \frac{J_1(\beta A)}{\beta A/2} [1+(\alpha-1)e^{-\alpha T}] J_o(\beta R)\beta d\beta . \tag{31}$$

For axial symmetry, the shear stress is zero, and the radial and tangential stresses are determined by

$$\sigma_r = -\frac{2Gz}{1-\nu}\left[\frac{\partial^2 w}{\partial r^2} + \frac{\nu}{r}\frac{\partial w}{\partial r}\right] \qquad (32a)$$

$$\sigma_\theta = -\frac{2Gz}{1-\nu}\left[\nu\frac{\partial^2 w}{\partial r^2} + \frac{1}{r}\frac{\partial w}{\partial r}\right] . \qquad (32b)$$

It is more convenient to consider the average sum and difference which, when introducing $R=r/\ell$, become

$$\frac{(\sigma_\theta+\sigma_r)}{2} = -\frac{2Gz}{2(1-\nu)}\frac{(1+\nu)}{\ell^2}\left[\frac{\partial^2 w}{\partial R^2} + \frac{1}{R}\frac{\partial w}{\partial R}\right] \qquad (33a)$$

$$\frac{(\sigma_\theta-\sigma_r)}{2} = -\frac{2Gz}{2(1-\nu)}\frac{(1-\nu)}{\ell^2}\left[-\frac{\partial^2 w}{\partial R^2} + \frac{1}{R}\frac{\partial w}{\partial R}\right] . \qquad (33b)$$

In this form Poisson's ratio ν is a factor in front of the differential operators. Furthermore, $(\sigma_\theta+\sigma_r)/2$ is the center of Mohr's circle for two-dimensional stress, and $(\sigma_\theta-\sigma_r)/2$ is the radius of Mohr's circle. This form facilitates superposition of stresses when more than one load is applied to the ice sheet.

We now substitute $2G = E_o D_T$ (equation 11a) into equation 33, and take the two-sided Laplace transform to obtain

$$\frac{\overline{\sigma}_\theta+\overline{\sigma}_r}{2(1+\nu)} = -\frac{E_o z}{2(1-\nu)}\frac{\overline{D}_T}{\ell^2}\left[\frac{\partial^2 \overline{w}}{\partial R^2} + \frac{1}{R}\frac{\partial \overline{w}}{\partial R}\right] \qquad (34a)$$

$$\frac{\overline{\sigma}_\theta-\overline{\sigma}_r}{2(1-\nu)} = -\frac{E_o z}{2(1-\nu)}\frac{\overline{D}_T}{\ell^2}\left[-\frac{\partial^2 \overline{w}}{\partial R^2} + \frac{1}{R}\frac{\partial \overline{w}}{\partial R}\right] . \qquad (34b)$$

By taking $\overline{D}_T$ inside the differentiation with respect to R, we see that we need $\overline{D}_T\,\overline{w}$. Multiplying equation 27 by $\overline{D}_T$ we obtain

$$\overline{D}_T\,\overline{w} = \frac{P}{2\pi k\ell^2}\int_o^\infty \frac{J_1(\beta A)}{\beta A/2}\left[\frac{\overline{D}_T}{s(1+\overline{D}_T\beta^4)}\right] J_o(\beta R)\beta d\beta . \qquad (35)$$

We need to take the derivatives of $\overline{D}_T \, \overline{w}$ according to equations 34. To do this we need the formulas

$$\frac{\partial}{\partial R} J_o(\beta R) = - \beta J_1(\beta R) \tag{36a}$$

$$\frac{\partial^2}{\partial R^2} J_o(\beta R) = \beta^2 \left[\frac{J_1(\beta R)}{\beta R} - J_o(\beta R)\right] . \tag{36b}$$

Using these relations equations 34 become

$$\frac{\overline{\sigma}_\theta+\overline{\sigma}_r}{2(1+\nu)} = \frac{P E_o z}{4\pi k \ell^4(1-\nu)} \int_o^\infty \frac{J_1(\beta A)}{\beta A/2} \left[\frac{\overline{D}_T}{s(1+\overline{D}_T\beta^4)}\right] J_o(\beta R)\beta^3 d\beta . \tag{37a}$$

$$\frac{\overline{\sigma}_\theta-\overline{\sigma}_r}{2(1-\nu)} = \frac{P E_o z}{4\pi k \ell^4(1-\nu)} \int_o^\infty \frac{J_1(\beta A)}{\beta A/2} \left[\frac{\overline{D}_T}{s(1+\overline{D}_T\beta^4)}\right] \frac{J_1(\beta R)}{\beta R/2} \beta^3 d\beta - \frac{\overline{\sigma}_\theta+\overline{\sigma}_r}{2(1+\nu)} . \tag{37b}$$

When E_o is not a function of z, the neutral axis is at the center of the ice sheet and ℓ^4, as defined by equation 13a, becomes

$$\ell^4 = \frac{E_o h^3}{12 \, k(1-\nu)} \tag{38}$$

where h is the ice thickness. For this case the maximum stress occurs at z=h/2 and part of the factor in front of the integral of equations 37 becomes

$$\frac{E_o z}{k\ell^4(1-\nu)} = \frac{6}{h^2} . \tag{39}$$

For the general case when E_o is a function of z, let us define C as

$$\frac{E_o z}{k\ell^4(1-\nu)} = \frac{6}{h^2} C , \tag{40}$$

where C represents a factor which corrects the solution if the material constants are a function of z. When the material constants are independent of z, C=1. Substituting equation 40 into equations 37, we obtain

$$\frac{(\bar{\sigma}_\theta+\bar{\sigma}_r)h^2}{2PC(1+\nu)} = \frac{3}{2\pi}\int_0^\infty \frac{J_1(\beta A)}{\beta A/2}\left[\frac{\bar{D}_T}{s(1+\bar{D}_T\beta^4)}\right] J_o(\beta R)\,\beta^3\,d\beta \tag{41a}$$

$$\frac{(\bar{\sigma}_\theta-\bar{\sigma}_r)h^2}{2PC(1-\nu)} = \frac{3}{2\pi}\int_0^\infty \frac{J_1(\beta A)}{\beta A/2}\left[\frac{\bar{D}_T}{s(1+\bar{D}_T\beta^4)}\right] \frac{J_1(\beta R)}{\beta R/2}\,\beta^3\,d\beta - \frac{(\bar{\sigma}_\theta+\bar{\sigma}_r)h^2}{2PC(1+\nu)}\,. \tag{41b}$$

Using the definition of $\bar{D}_T = s/(1+s)$, the s factor of equation 41 becomes

$$\frac{\bar{D}_T}{s(1+\bar{D}_T\beta^4)} = \frac{\alpha}{s+\alpha}\,, \tag{42}$$

whose inverse is easily obtained from equation 18b. Hence equations 41 become

$$\frac{(\sigma_\theta+\sigma_r)h^2}{2PC(1+\nu)} = \frac{3H(T)}{2\pi}\int_0^\infty \frac{J_1(\beta A)}{\beta A/2}\,[\alpha e^{-\alpha T}]\,J_o(\beta R)\beta^3\,d\beta \tag{43a}$$

$$\frac{(\sigma_\theta-\sigma_r)h^2}{2PC(1-\nu)} = \frac{3H(T)}{2\pi}\int_0^\infty \frac{J_1(\beta A)}{\beta A/2}\,[\alpha e^{-\alpha T}]\,\frac{J_1(\beta R)}{\beta R/2}\,\beta^3\,d\beta - \frac{(\sigma_\theta+\sigma_r)h^2}{2PC(1+\nu)}\,. \tag{43b}$$

Hence, for secondary creep we have obtained the deflection in equation 31 and the stresses in equations 43. Let us now discuss the convergence of these integrals as β approaches ∞. First the Bessel functions $J_o(\beta R)$ and $J_1(\beta A)$ each approach $1/\sqrt{\beta}$ as β becomes large. The worst case is when A=0 and R=0. In this case $J_1(\beta A)/(\beta A/2)=1$ and $J_o(\beta R)=1$. As β becomes large α approaches $1/\beta^4$. This means $e^{-\alpha T}$ approaches 1. Hence the integrand of the deflection integral approaches $1/\beta^3$ which shows that the deflection integral is convergent for large β.

The stress integrals in equations 43a and 43b converge when $A \neq 0$ and/or $R \neq 0$. When both A=0 and R=0 equation 43a diverges because the integrand goes to $1/\beta$ for large β. When A=0, equation 43b is discontinuous at R=0.

The divergence of equation 43a and the discontinuity of equation 43b, when both A=0 and R=0, is really associated with the elastic component obtained when T=0. Let us substract from the stresses in equations 43 their respective elastic parts obtained when T=0. Let us use a superscript * to denote this new stress. Hence equations 43 become

$$\frac{(\sigma_\theta+\sigma_r)^* h^2}{2PC(1+\nu)} = \frac{3H(T)}{2\pi} \int_o^\infty \frac{J_1(\beta A)}{\beta A/2} \alpha[e^{-\alpha T} -1]\, J_o(\beta R)\beta^3\, d\beta \qquad (44a)$$

$$\frac{(\sigma_\theta-\sigma_r)^* h^2}{2PC(1-\nu)} = \frac{3H(T)}{2\pi} \int_o^\infty \frac{J_1(\beta A)}{\beta A/2} \alpha[e^{-\alpha T} -1]\, \frac{J_1(\beta R)}{\beta R/2}\beta^3\, d\beta - \frac{(\sigma_\theta+\sigma_r)^* h^2}{2PC(1+\nu)}\,. \qquad (44b)$$

These new integrals go to $1/\beta^5$ as β becomes large, and hence, are convergent and continuous when both A=0 and R=0.

For numerical computation it also is convenient to consider the deflection equation minus its elastic deflection. This equation is

$$\frac{w^{*}k\ell^{2}}{P} = \frac{H(T)}{2\pi} \int_{0}^{\infty} \frac{J_{1}(\beta A)}{\beta A/2} (\alpha-1)(e^{-\alpha T}-1)\, J_{o}(\beta R)\, \beta d\beta \ . \tag{45}$$

The integrand of this integral still approaches $1/\beta^{3}$ for large β, and nothing is gained for the convergence rate. However, there is a close similarity to equation 44a.

The concept of subtracting the elastic part at T=0 from the integrals is new and provides a method for easily evaluating the time-dependent part of the integrals. It has further significance on the influence of the load distribution parameter "A" as is shown later.

The elastic parts of these integrals have already been developed. Following Wyman's solution they are, for R>A:

$$\frac{w^{0}k\ell^{2}}{P} = \frac{1}{\pi A} \,[\mathrm{ber}'A \ \mathrm{ker}\ R - \mathrm{bei}'A\ \mathrm{kei}\ R], \tag{46}$$

$$\frac{(\sigma_{\theta}+\sigma_{r})^{0}h^{2}}{2PC(1+\nu)} = \frac{3}{\pi A} \,[\mathrm{ber}'A\ \mathrm{kei}\ R + \mathrm{bei}'A\ \mathrm{ker}\ R]\ , \tag{47a}$$

$$\frac{(\sigma_{\theta}-\sigma_{r})^{0}h^{2}}{2PC(1-\nu)} = \frac{3}{\pi A}\,\frac{2}{R}\,[-\mathrm{ber}'A\ \mathrm{ker}'R + \mathrm{bei}'A\ \mathrm{kei}'R] - \frac{(\sigma_{\theta}+\sigma_{r})^{0}h^{2}}{2PC(1+\nu)}\ . \tag{47b}$$

And for R < A:

$$\frac{w^{0}k\ell^{2}}{P} = \frac{1}{\pi A}\,[\frac{1}{A} + \mathrm{ker}'A\ \mathrm{ber}\ R - \mathrm{kei}'A\ \mathrm{bei}\ R]\ , \tag{48}$$

$$\frac{(\sigma_{\theta}+\sigma_{r})^{0}h^{2}}{2PC(1+\nu)} = \frac{3}{\pi A}\,[\mathrm{ker}'A\ \mathrm{bei}\ R + \mathrm{kei}'A\ \mathrm{ber}\ R]\ , \tag{49a}$$

$$\frac{(\sigma_\theta - \sigma_r)^0 h^2}{2PC(1-\nu)} = \frac{3}{\pi A}\ \frac{2}{R}\,[-\mathrm{ker}'A\ \mathrm{ber}'R + \mathrm{kei}'A\ \mathrm{bei}'R] - \frac{(\sigma_\theta + \sigma_r)^0 h^2}{2PC(1+\nu)}. \qquad (49b)$$

In these equations the superscript zero means the elastic part for T=0. The prime on a Kelvin function represents its first derivative.

SECONDARY CREEP FOR A CONCENTRATED LOAD

Let us now consider the secondary creep for a concentrated load, A=0. Then equation 45 and equations 44, with R and T as parameters, reduce to

$$\frac{w^{*}k\ell^{2}}{P} = \frac{-H(T)}{2\pi}\int_{0}^{\infty} \frac{[e^{-T/(1+\beta^{4})}-1]}{1+\beta^{4}} J_{0}(\beta R)\,\beta^{5}\,d\beta\,, \qquad (50)$$

$$\frac{(\sigma_{\theta}+\sigma_{r})^{*}h^{2}}{2PC(1+\nu)} = \frac{3H(T)}{2\pi}\int_{0}^{\infty} \frac{[e^{-T/(1+\beta^{4})}-1]}{1+\beta^{4}} J_{0}(\beta R)\,\beta^{3}\,d\beta\,, \qquad (51a)$$

$$\frac{(\sigma_{\theta}-\sigma_{r})^{*}h^{2}}{2PC(1-\nu)} = \frac{3H(T)}{2\pi}\int_{0}^{\infty} \frac{[e^{-T/(1+\beta^{4})}-1]}{1+\beta^{4}} \frac{J_{1}(\beta R)}{\beta R/2}\,\beta^{3}\,d\beta - \frac{(\sigma_{\theta}+\sigma_{r})^{*}h^{2}}{2PC(1+\nu)}\,. \qquad (51b$$

The elastic parts for A=0 are

$$\frac{w^{0}k\ell^{2}}{P} = -\frac{1}{2\pi}\,\mathrm{kei}\,R, \qquad (52)$$

$$\frac{(\sigma_{\theta}+\sigma_{r})^{0}h^{2}}{2PC(1+\nu)} = \frac{3}{2\pi}\,\mathrm{ker}\,R\,, \qquad (53a)$$

$$\frac{(\sigma_{\theta}-\sigma_{r})^{0}h^{2}}{2PC(1-\nu)} = \frac{3}{2\pi}\left[\frac{2}{R}\,\mathrm{kei}'R - \mathrm{ker}\,R\right]. \qquad (53b)$$

Taking the limit as R approaches zero in equation 53b gives a finite value of $3/4\pi$.

The integrals in equations 50 and 51 were numerically evaluated up to $\beta = 10$. For the remainder of the integrals from 10 to ∞, the following approximation was made

$$\frac{e^{-T/(1+\beta^{4})}-1}{1+\beta^{4}} \simeq \frac{-T}{(1+\beta^{4})^{2}} + \frac{T^{2}/2}{(1+\beta^{4})^{3}} + \mathcal{O}(\beta^{-16})\,. \qquad (54a)$$

Expanding $1/(1+\beta^4)$ we obtain

$$\frac{e^{-T/(1+\beta^4)}-1}{1+\beta^4} \simeq \frac{-T}{\beta^8} + \frac{2T+T^2/2}{\beta^{12}} + \mathcal{O}(\beta^{-16}) \tag{54b}$$

I. M. Longman [63] gives a recurrance relation for integrals of the type

$$\int_x^\infty J_o(\beta) \quad \beta^{-n}\, d\beta \quad \text{and} \int_x^\infty J_1(\beta)\, \beta^{-n}\, d\beta \; .$$

From these relations, the above integrals from 10 to ∞ can be expressed in terms of $\int_x^\infty J_o(\beta)\, \beta^{-1}\, d\beta$ for which computational methods are given in reference [64]. Computations were made for T = 2, 5 and 10 when R goes in increments of 0.1 from R=0 to R=5. The results are tabulated in Tables 1, 2, and 3. In order to obtain the actual profile, the elastic part as given by equations 52 and 53 was added. These results are shown in Figures 9, 10, and 11. In Figure 9 we observe that the maximum upward deflection increases with time and moves closer to the load. This feature has been observed in field tests by G. Frankenstein [32]. Vaudrey and Katona [56] have predicted deflection profiles by finite element methods which do not show this feature. This is probably due to assuming a finite boundary rather than an infinite one.

From these figures we see that the maximum deflection and stresses occur at R=0. Let us now consider these maximums as a function of the load radius A.

Table 1. $\frac{w^{*}k\ell^{2}}{P}$ for Secondary Creep when a A=0.

R	T=2.	T=5.	T=10.
0	.101 637	.206 665	.332 334
.1	.099 197	.200 754	.320 982
.2	.094 074	.188 556	.297 894
.3	.087 492	.173 102	.269 124
.4	.080 075	.155 929	.237 689
.5	.072 232	.138 032	.205 501
.6	.064 253	.120 099	.173 847
.7	.056 349	.102 619	.143 607
.8	.048 676	.085 940	.115 374
.9	.041 348	.070 303	.089 523
1.0	.034 445	.055 868	.066 270
1.1	.028 024	.042 730	.045 704
1.2	.022 120	.030 935	.027 823
1.3	.016 750	.020 489	.012 552
1.4	.011 920	.011 368	.000 235
1.5	.007 625	.003 524	.010 702
1.6	.003 851	-.003 108	-.019 037
1.7	.000 577	-.008 606	-.025 441
1.8	-.002 223	-.013 056	-.030 125
1.9	-.004 577	-.016 550	-.033 298
2.0	-.006 517	-.019 181	-.035 163
2.1	-.008 075	-.021 043	-.035 917
2.2	-.009 287	-.022 228	-.035 745
2.3	-.010 184	-.022 825	-.034 816
2.4	-.010 801	-.022 919	-.033 287
2.5	-.011 170	-.022 589	-.031 299
2.6	-.011 323	-.021 909	-.028 976
2.7	-.011 288	-.020 947	-.026 428
2.8	-.011 094	-.019 765	-.023 750
2.9	-.010 767	-.018 419	-.021 023
3.0	-.010 330	-.016 958	-.018 312
3.1	-.009 806	-.015 424	-.015 672
3.2	-.009 214	-.013 856	-.013 148
3.3	-.008 574	-.012 286	-.010 771
3.4	-.007 900	-.010 741	-.008 567
3.5	-.007 207	-.009 242	-.006 551
3.6	-.006 507	-.007 809	-.004 732
3.7	-.005 811	-.006 455	-.003 115
3.8	-.005 128	-.005 190	-.001 698
3.9	-.004 465	-.004 022	-.000 476
4.0	-.003 829	-.002 956	.000 558
4.1	-.003 225	-.001 993	.001 417
4.2	-.002 656	-.001 133	.002 112
4.3	-.002 126	-.000 376	.002 658
4.4	-.001 635	.000 282	.003 067
4.5	-.001 186	.000 845	.003 356
4.6	-.000 778	.001 318	.003 576
4.7	-.000 411	.001 707	.003 629
4.8	-.000 085	.002 018	.003 640
4.9	.000 201	.002 258	.003 587
5.0	.000 450	.002 433	.003 479

Table 2. $\frac{(\sigma_\theta+\sigma_r)^* h^2}{2PC(1+\nu)}$ for Secondary Creep when A=0

R	T=2.	T=5.	T=10.
0	-.157 475	-.261 150	-.343 751
.1	-.156 719	-.259 613	-.341 284
.2	-.154 495	-.255 116	-.334 099
.3	-.150 914	-.247 916	-.322 684
.4	-.146 114	-.238 342	-.307 643
.5	-.140 252	-.226 751	-.289 631
.6	-.133 491	-.213 514	-.269 308
.7	-.125 994	-.198 995	-.247 310
.8	-.117 923	-.183 545	-.224 232
.9	-.109 428	-.167 490	-.200 617
1.0	-.100 654	-.151 130	-.176 946
1.1	-.091 733	-.134 732	-.153 637
1.2	-.082 784	-.118 536	-.131 043
1.3	-.073 914	-.102 743	-.109 454
1.4	-.065 217	-.087 529	-.089 099
1.5	-.056 775	-.073 033	-.070 153
1.6	-.048 655	-.059 369	-.052 737
1.7	-.040 916	-.046 622	-.036 928
1.8	-.033 601	-.034 853	-.022 760
1.9	-.026 746	-.024 100	-.010 236
2.0	-.020 376	-.014 381	.000 676
2.1	-.014 506	-.005 696	.010 028
2.2	-.009 146	.001 969	.017 895
2.3	-.004 296	.008 643	.024 365
2.4	.000 049	.014 364	.029 538
2.5	.003 900	.019 179	.033 524
2.6	.007 272	.023 141	.036 434
2.7	.010 183	.026 310	.038 381
2.8	.012 657	.028 747	.039 480
2.9	.014 717	.030 516	.039 841
3.0	.016 390	.031 682	.039 569
3.1	.017 704	.032 311	.038 766
3.2	.018 686	.032 463	.037 525
3.3	.019 367	.032 203	.035 935
3.4	.019 773	.031 586	.034 073
3.5	.019 935	.030 670	.032 012
3.6	.019 878	.029 507	.029 814
3.7	.019 631	.028 144	.027 536
3.8	.019 187	.026 626	.025 226
3.9	.018 650	.024 994	.022 926
4.0	.017 993	.023 284	.020 670
4.1	.017 224	.021 528	.018 485
4.2	.016 378	.019 756	.016 395
4.3	.015 473	.017 991	.014 415
4.4	.014 526	.016 255	.012 561
4.5	.013 551	.014 567	.010 838
4.6	.012 563	.012 941	.009 253
4.7	.011 573	.011 388	.007 807
4.8	.010 591	.009 919	.006 498
4.9	.009 627	.008 540	.005 324
5.0	.008 688	.007 255	.004 281

Table 3. $\frac{(\sigma_\theta - \sigma_r)^* h^2}{2PC(1-\nu)}$ for Secondary Creep when A=0

R	T=2.	T=5.	T=10.
0	.000	.000	.000
.1	-.000 378	-.000 767	-.001 230
.2	-.001 480	-.002 993	-.004 780
.3	-.003 238	-.006 514	-.010 340
.4	-.005 563	-.011 125	-.017 530
.5	-.008 357	-.016 602	-.025 948
.6	-.011 512	-.022 720	-.035 194
.7	-.014 956	-.029 259	-.044 893
.8	-.018 565	-.036 016	-.054 700
.9	-.022 260	-.042 802	-.064 313
1.0	-.025 960	-.049 451	-.073 473
1.1	-.029 590	-.055 819	-.081 968
1.2	-.033 088	-.061 784	-.089 628
1.3	-.036 396	-.067 247	-.096 326
1.4	-.039 471	-.072 130	-.101 977
1.5	-.042 272	-.076 376	-.106 529
1.6	-.044 773	-.079 946	-.109 963
1.7	-.046 950	-.082 820	-.112 289
1.8	-.048 790	-.084 991	-.113 539
1.9	-.050 286	-.086 468	-.113 765
2.0	-.051 436	-.087 271	-.113 035
2.1	-.052 244	-.087 427	-.111 428
2.2	-.052 719	-.086 975	-.109 032
2.3	-.052 873	-.085 957	-.105 941
2.4	-.052 722	-.084 423	-.102 249
2.5	-.052 284	-.082 423	-.098 053
2.6	-.051 581	-.080 011	-.093 449
2.7	-.050 633	-.077 242	-.088 526
2.8	-.049 465	-.074 171	-.083 371
2.9	-.048 100	-.070 849	-.078 064
3.0	-.046 563	-.067 329	-.072 691
3.1	-.044 877	-.063 661	-.067 287
3.2	-.043 066	-.059 890	-.061 944
3.3	-.041 154	-.056 060	-.056 702
3.4	-.039 163	-.052 211	-.051 607
3.5	-.037 112	-.048 379	-.046 696
3.6	-.035 024	-.044 596	-.042 000
3.7	-.032 915	-.040 891	-.037 544
3.8	-.030 803	-.037 288	-.033 344
3.9	-.028 703	-.033 810	-.029 415
4.0	-.026 630	-.030 472	-.025 762
4.1	-.024 596	-.027 291	-.022 389
4.2	-.022 613	-.024 276	-.019 295
4.3	-.020 689	-.021 436	-.016 475
4.4	-.018 833	-.018 776	-.013 922
4.5	-.017 052	-.016 300	-.011 626
4.6	-.015 352	-.014 008	-.009 576
4.7	-.013 736	-.011 899	-.007 757
4.8	-.012 209	-.009 970	-.006 156
4.9	-.010 771	-.008 216	-.004 758
5.0	-.009 424	-.006 632	-.003 548

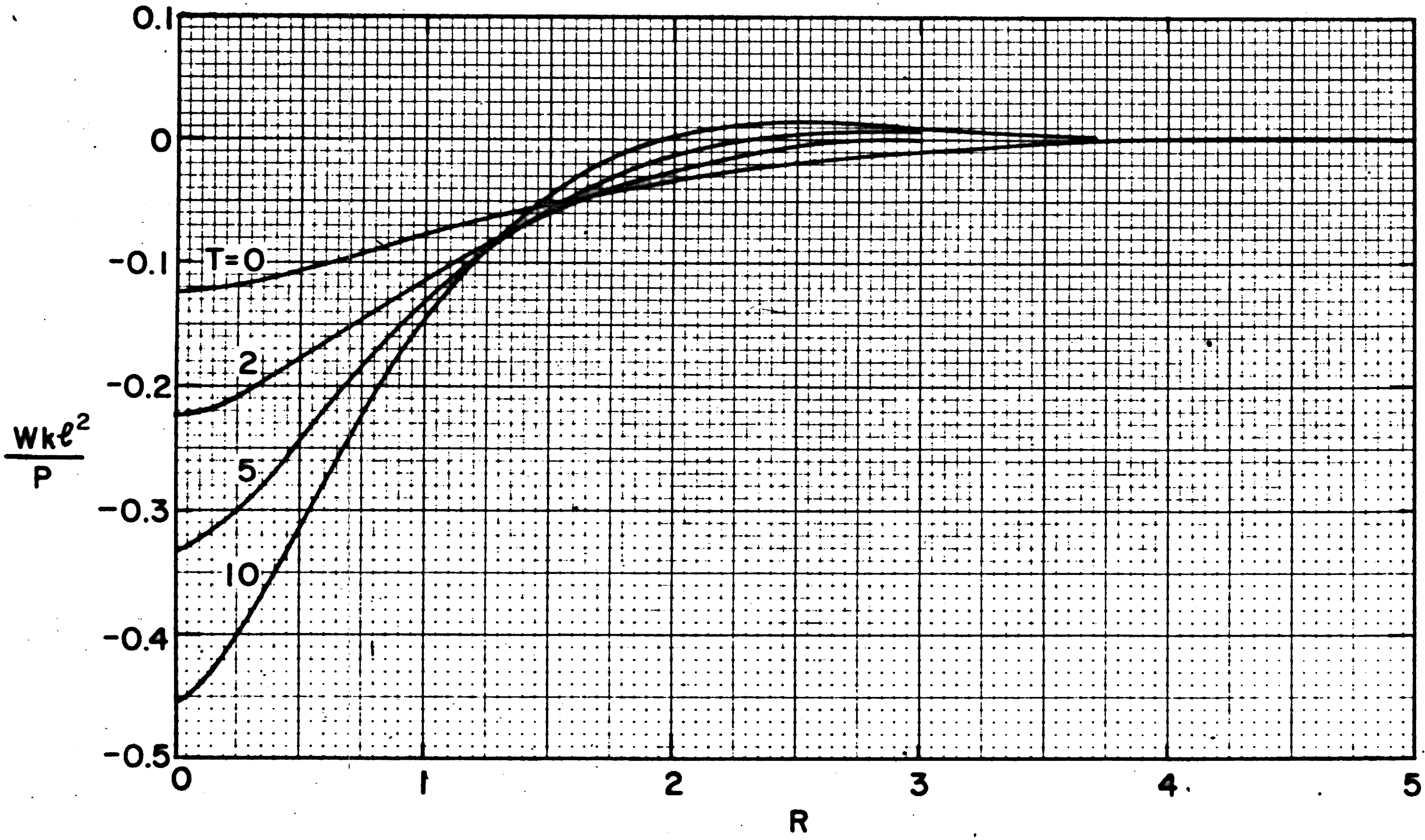

Figure 9. Secondary creep deflection profile for a concentrated load.

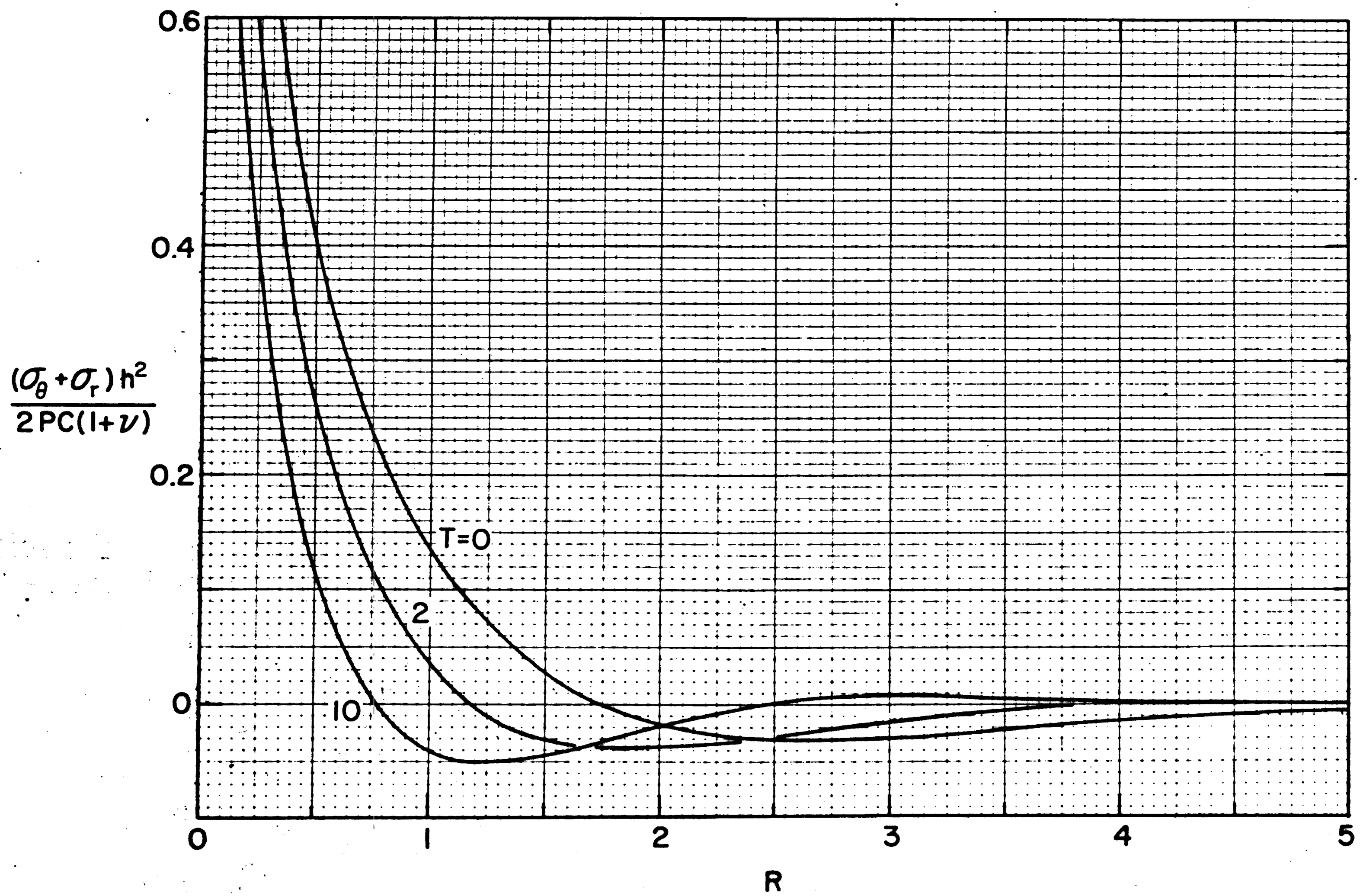

Figure 10. Secondary creep stress $\sigma_\theta + \sigma_r$ profile for a concentrated load.

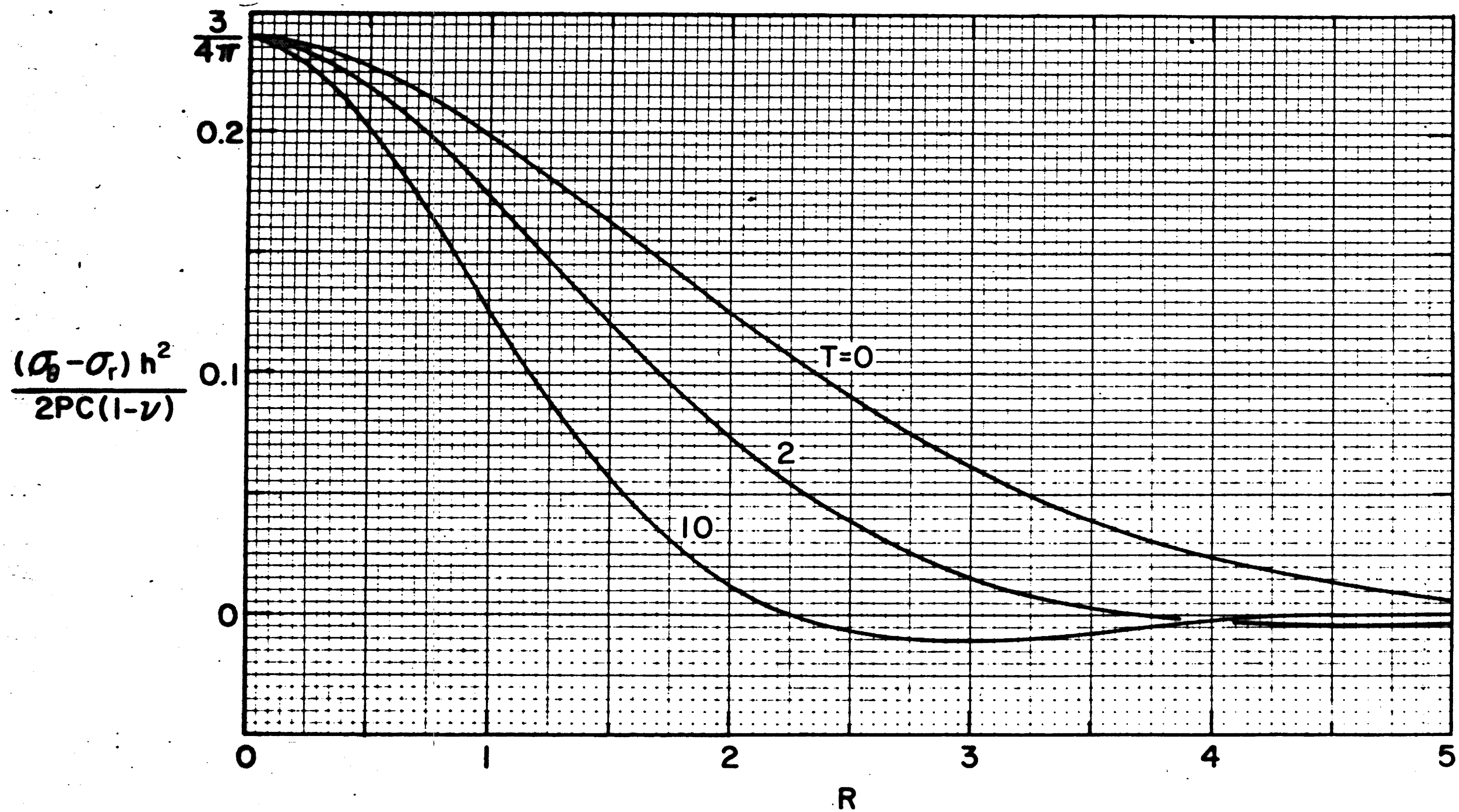

Figure 11. Secondary creep stress σ_θ-σ_r profile for a concentrated load.

The equations 45 and 44a for R=0 reduce to

$$\frac{w^* k\ell^2}{P} = -\frac{H(T)}{2\pi}\int_0^\infty \frac{[e^{-T/(1+\beta^4)}-1]}{1+\beta^4}\ \frac{J_1(\beta A)}{\beta A/2}\ \beta^5\, d\beta\ , \tag{55}$$

$$\frac{(\sigma_\theta+\sigma_r)^* h^2}{2PC(1+\nu)} = \frac{3H(T)}{2\pi}\int_0^\infty \frac{[e^{-T/(1+\beta^4)}-1]}{1+\beta^4}\ \frac{J_1(\beta A)}{\beta A/2}\ \beta^3\, d\beta\ , \tag{56a}$$

while equation 44b becomes

$$\frac{(\sigma_\theta-\sigma_r)^* h^2}{2PC(1-\nu)} = 0\ . \tag{56b}$$

The corresponding elastic parts for this case are

$$\frac{w^0 k\ell^2}{P} = \frac{1}{\pi A}\ [\frac{1}{A} + \mathrm{ker}'A]\ , \tag{57}$$

$$\frac{(\sigma_\theta+\sigma_r)^0 h^2}{2PC(1+\nu)} = \frac{3}{\pi A}\ \mathrm{kei}'A\ , \tag{58a}$$

$$\frac{(\sigma_\theta-\sigma_r)^0 h^2}{2PC(1-\nu)} = 0\ . \tag{58b}$$

Note that the elastic stress $(\sigma_\theta-\sigma_r)^0 h^2/[2PC(1-\nu)]$ has a discontinuity at R=0 when A=0. If A=0 first and R approaches 0 second, this stress becomes $3/4\pi$. On the other hand if R=0 first, this stress be= comes 0. This can be explained by the fact that when A=0 first, the stress is being evaluated at the edge of the concentrated load, but when R=0 first the stress is being evaluated directly under the center of the concentrated load. Since the thin-plate theory does not predict correct stresses in the vicinity of relatively concentrated loads, the elastic layer solution must be used to obtain the correct answer which is 0.

The procedure for numerical integrating equations 55 and 56 is the same as for equations 50 and 51. Numerical computations were made for T=2, 5 and 10 when A goes in increments of 0.1 from A=0 to A=2. The values for equations 55 and 56a are tabulated in Tables 4 and 5 respectively. The results show that for constant time, the value of the result for any A is not significantly different from the value at A=0 if A is not too large. The relative error for the deflection is $[w^*(A)-W^*(0)]/w^*(0)$ and this is shown in Figure 12 for T=2, 5 and 10. This small relative error is not too surprising, since the elastic deflections do not significantly depend on A for small A. The relative error for the stress of equation 56a is also shown in Figure 12. This error is even less than the one for the deflections. For the elastic case this stress significantly depends on A as can be from the elastic stress formula for small A which is

$$\frac{(\sigma_\theta+\sigma_r)^2 h^2}{2PC(1+\nu)} = \frac{3}{2\pi} \; [0.5 - \gamma - \log\,(A/2)] \tag{59}$$

where $\gamma = 0.5772\ldots$ which is Euler's Number.

For practical application A is usually small. For a 12-inch thick ice sheet with E_o=7000 kgf/cm^2 and ν=1/2, the flexural rigidity length ℓ is about 14 feet. For thicker ice sheets ℓ is even greater. The largest radius of loading that a pneumatic tire would produce is about one foot. Hence, A=1/14, for which the error for the stress is much less than 1%.

This result is extremely important because it allows us to compute the time dependent asterisked stress for A=0. To this we can add the elastic stresses for A≠0.

Table 4. $\frac{w^* k\ell^2}{P}$ for Secondary Creep When R=0

A	T=2.	T=5.	T=10.
0	.101 637	.206 650	.332 334
.1	.100 317	.203 454	.326 162
.2	.097 460	.196 614	.313 139
.3	.093 679	.187 667	.296 325
.4	.089 294	.177 401	.277 278
.5	.084 519	.166 340	.257 018
.6	.079 509	.154 862	.236 267
.7	.074 383	.143 246	.215 554
.8	.069 231	.131 708	.195 266
.9	.064 126	.120 409	.175 688
1.0	.059 124	.109 474	.157 027
1.1	.054 268	.098 993	.139 424
1.2	.049 591	.089 033	.122 971
1.3	.045 118	.079 639	.107 720
1.4	.040 867	.070 840	.093 690
1.5	.036 850	.062 650	.080 878
1.6	.033 079	.055 073	.069 258
1.7	.029 545	.048 102	.058 789
1.8	.026 259	.041 724	.049 420
1.9	.023 214	.035 921	.041 091
2.0	.020 406	.030 669	.033 737

Table 5. $\frac{(\sigma_\theta+\sigma_r)^* h^2}{2PC(1+\nu)}$ for Secondary Creep when R=0

A	T=2.	T=5.	T=10.
0	-.157 475	-.261 150	-.343 751
.1	-.157 096	-.260 378	-.342 514
.2	-.155 975	-.258 108	-.338 879
.3	-.154 151	-.254 430	-.333 023
.4	-.151 677	-.249 466	-.325 173
.5	-.148 609	-.243 353	-.315 579
.6	-.145 012	-.236 234	-.304 502
.7	-.140 950	-.228 255	-.292 202
.8	-.136 488	-.219 561	-.278 932
.9	-.131 688	-.210 292	-.264 930
1.0	-.126 614	-.200 581	-.250 419
1.1	-.121 324	-.190 552	-.235 605
1.2	-.115 872	-.180 320	-.220 671
1.3	-.110 311	-.169 990	-.205 780
1.4	-.104 688	-.159 658	-.191 076
1.5	-.099 047	-.149 408	-.176 682
1.6	-.093 428	-.139 315	-.162 700
1.7	-.087 865	-.129 442	-.149 216
1.8	-.082 391	-.119 845	-.136 299
1.9	-.077 032	-.110 569	-.124 001
2.0	-.071 812	-.101 652	-.112 359

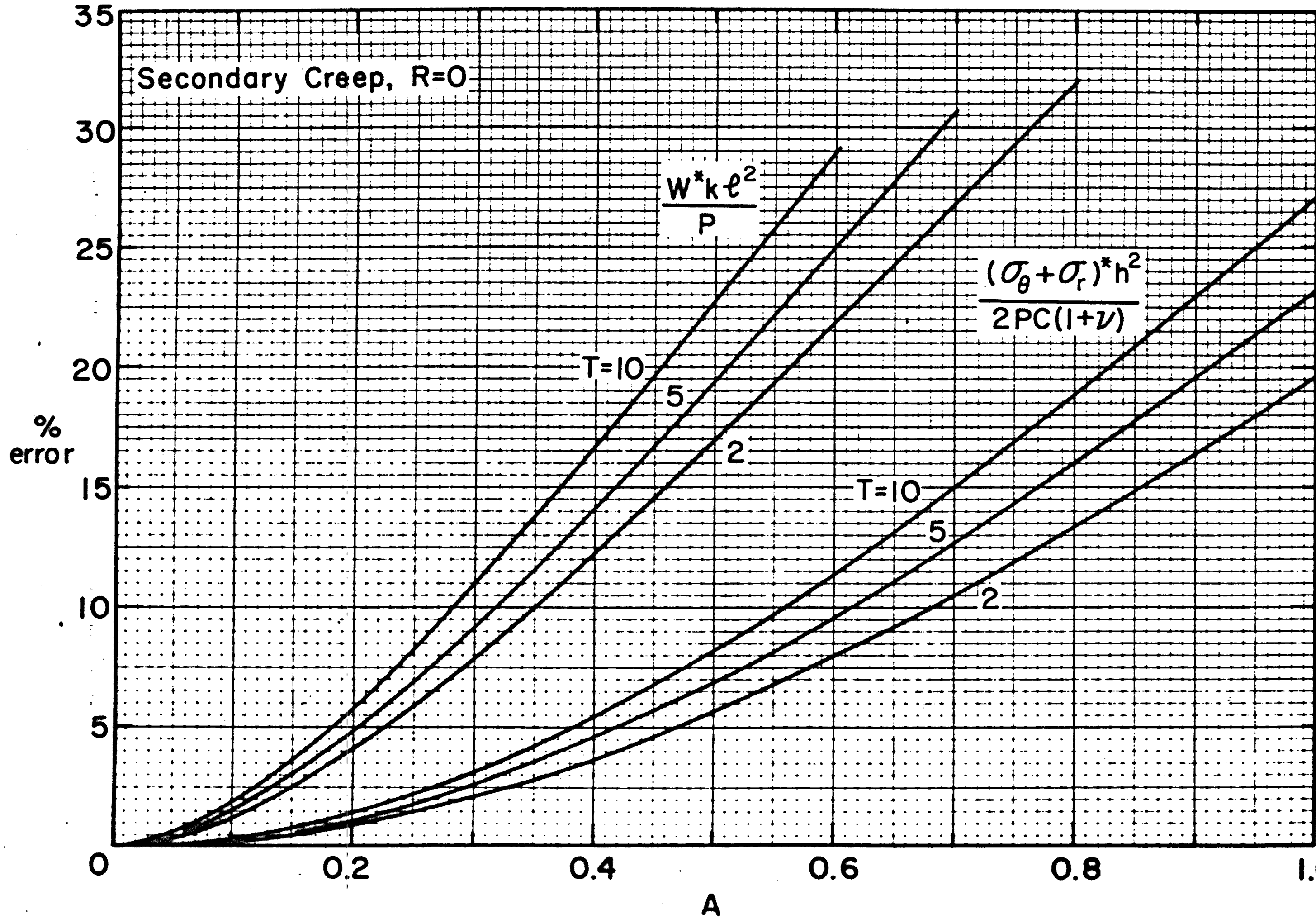

Figure 12. Percent error directly under the load for neglecting the radius "A" of the load distribution.

SECONDARY CREEP UNDER A CONCENTRATED LOAD

Since equations 55 and 56a do not significantly depend on A for small values of A, we can let A=0 and obtain

$$\frac{w^{*}k\ell^{2}}{P} = -\frac{H(T)}{2\pi}\int_{0}^{\infty}\frac{[e^{-T/(1+\beta^{4})}-1]}{1+\beta^{4}}\,\beta^{5}\,d\beta \tag{60a}$$

$$\frac{(\sigma_{\theta}+\sigma_{r})^{*}h^{2}}{2PC(1+\nu)} = \frac{3H(T)}{2\pi}\int_{0}^{\infty}\frac{[e^{-T/(1+\beta^{4})}-1]}{1+\beta^{4}}\,\beta^{3}\,d\beta\ . \tag{60b}$$

If we let

$$x = \frac{T}{1+\beta^{4}}\ , \tag{61}$$

these equations become

$$\frac{w^{*}k\ell^{2}}{P} = \frac{+H(T)}{8\pi}\int_{0}^{T}\frac{(1-e^{-x})}{x}\sqrt{\frac{T-x}{x}}\,dx\ , \tag{62a}$$

$$\frac{(\sigma_{\theta}+\sigma_{r})^{*}h^{2}}{2PC(1+\nu)} = -\frac{3H(T)}{8\pi}\int_{0}^{T}\frac{(1-e^{-x})}{x}\,dx\ , \tag{62b}$$

which are known integrals and can be written as

$$\frac{w^{*}k\ell^{2}}{P} = \frac{H(T)}{8}\,[-1+{}_{1}F_{1}(-.5,\ 1,\ -T)], \tag{63a}$$

$$\frac{(\sigma_{\theta}+\sigma_{r})^{*}h^{2}}{2PC(1+\nu)} = -\frac{3H(T)}{8\pi}\,[E_{1}(T)+\gamma+\log T]\ . \tag{63b}$$

The symbol ${}_{1}F_{1}(a,b,z)$ is the confluent hypergeometric function, $E_{1}(z)$ is the exponential function, and γ=0.5772 ... which is Euler's number. Since $w^{0}k\ell^{2}/P = H(T)/8$, it is more convenient to consider the total deflection w rather than w* in equation 63a. In reference [64], the series expansion and the asymptotic expansion of ${}_1F_1$ are given. Substituting these into equation 63a, we get for small T

$$\frac{wk\ell^2}{P} = \frac{H(T)}{8} \sum_{n=0} \frac{-(2n-3)!!}{2^n} \frac{(-T)^n}{(n!)^2}, \qquad (64a)$$

and for large T

$$\frac{wk\ell^2}{P} = \frac{H(T)\sqrt{T}}{4\sqrt{\pi}} \sum_{n=0}^{\infty} \frac{[2n-3)!!]^2}{2^{2n}\ n!\ T^n}, \qquad (64b)$$

where $(2n-3)!! = 1\cdot2\cdot3\cdots(2n-3)$. For the special cases when n equals 0 and 1, we have by definition $(-3)!! = -1$ and $(-1)!! = 1$. The series expansion for E_1 is

$$E_1(z) = -\gamma - \log z - \sum_{n=1}^{\infty} \frac{(-z)^n}{n\ n!}. \qquad (65a)$$

Reference [64] gives an accurate approximation for E_1 when the argument is large. However, it is also convenient to have a simple, less accurate approximation. The expression

$$E_1(z) = \frac{e^{-z}}{z}\left[\frac{z+0.309}{z+1.196}\right] \qquad (65b)$$

was developed for large arguments. The two constants were determined by forcing the equation through z equal to 1 and 2. This equation has a maximum error of 0.6% for $z>1$.

We now have developed rather simple formulas for the deflection and stress directly under a load for secondary creep. To the stresses we must still add the elastic stress from equation 58a. When A is small we know that this elastic stress is incorrect and we must consider the stress from the three dimensional elastic layer theory. We now pose the question, can we add the asterisked stress as given in equation 63b to the stress from the elastic layer theory for small A? We will not prove this statement in general but consider the special case when A=0. From reference [15] we can easily show that the elastic-layer theory for a concentrated load gives

$$\frac{(\sigma_\theta+\sigma_r)h^2}{2P(1+\nu)} = 0.830 - \frac{3}{2\pi} \log \frac{h}{(D/k)^{1/4}} . \tag{66}$$

Notice that for the elastic-layer solution, the properties were uniform and hence C=1. Substituting for $D/k = \ell^4 D_T$ and letting $P = PH(T)$ we get

$$\frac{\sigma_\theta+\sigma_r}{2(1+\nu)} = [0.830 - \frac{3}{2\pi} \log \frac{h}{\ell} + \frac{3}{8\pi} \log D_T] \frac{P}{h^2} H(T) . \tag{67}$$

Using E.H. Lee's correspondence principle, we obtain for the Laplace transform of the solution

$$\frac{\overline{\sigma}_\theta+\overline{\sigma}_r}{2(1+\nu)} = [0.830 - \frac{3}{2\pi} \log \frac{h}{\ell} + \frac{3}{8\pi} \log \overline{D}_T] \frac{P}{sh^2} , \tag{68}$$

where $\overline{D}_T = s/(I+s)$.

From reference [65], formula 5.7(5), we have

$$\overline{H(T)E_1(T)} = \frac{\log(s+1)}{s} , \tag{68}$$

and from formula 5.7(1)

$$\overline{-H(T)(\gamma+\log T)} = \frac{\log s}{s} . \qquad (69b)$$

Hence the inverse of equation 68 becomes

$$\frac{(\sigma_\theta+\sigma_r)h^2}{2P(1+\nu)} = H(T)\ [0.830 - \frac{3}{2\pi}\log\frac{h}{\ell}]$$
$$- \frac{3H(T)}{8\pi}\ [E_1(T) + \gamma + \log T] . \qquad (70)$$

The first part of equation 70 is the elastic layer part for time zero. The second part is the same as equation 63b. Therefore we have proved that for A=0, the asterisked stress of equation 63b can be added to the elastic layer solution to obtain the time dependent solution. When "A" is small but not zero, we would expect the same procedure to be valid.

For primary creep equation 8 reduces to

$$\frac{1}{2G} = \frac{1}{E_1} + \frac{1}{\eta_o \partial/\partial t} + \frac{1}{E_2+\eta_2\partial/\partial t} \,. \tag{71}$$

We let $2G = E_o\, D_T$ with $T = E_o t/\eta_o$ as before, but now

$$D_T = \frac{\partial/\partial T\ (\tau+\ \partial/\partial T)}{E\ \partial^2/\partial T^2+(1+\tau)\ \partial/\partial T + \tau} , \tag{72}$$

where

$$E = E_o/E_1, \tag{73a}$$

and

$$\tau = (\eta_o E_2)/(E_o \eta_2). \tag{73b}$$

Note that $0 \leqslant \tau \leqslant \infty$ and $0 \leqslant E \leqslant 1$. We proceed exactly as we did for secondary creep, except now

$$\bar{D}_T = \frac{s(\tau+s)}{E\ s^2+\ (1+\tau)s + \tau} \,. \tag{74}$$

The "s" factor in equation 27 now becomes, with the use of partial fractions

$$\frac{1}{s}\,\frac{1}{1+\bar{D}_T\beta^4} = \frac{1}{s} + \frac{\beta^4}{(E+\beta^4)(\alpha_2-\alpha_1)}\left[\frac{\tau-\alpha_2}{s+\alpha_2} - \frac{\tau-\alpha_1}{s+\alpha_1}\right], \tag{75}$$

where

$$\alpha_1 = \frac{(1+\tau+\tau\beta^4) - [(1+\tau+\tau\beta^4)^2 - 4\tau(E+\beta^4)]^{1/2}}{2(E+\beta^4)} , \tag{76a}$$

$$\alpha_2 = \frac{(1+\tau+\tau\beta^4) + [(1+\tau+\tau\beta^4)^2 - 4\tau(E+\beta^4)]^{1/2}}{2(E+\beta^4)} , \tag{76b}$$

which are always positive. We note that α_1 and α_2 are the negative values of the roots of

$$(E+\beta^4)s^2 + (1+\tau+\tau\beta^4)s + \tau = 0 \,. \tag{77}$$

Using equation 18b, the inverse Laplace transform of equation 27 becomes

$$\frac{wk\ell^2}{P} = \frac{H(T)}{2\pi}\int_0^\infty \frac{J_1(\beta A)}{\beta A/2}\left[1 + \frac{\beta^4[(\tau-\alpha_2)e^{-\alpha_2 T}-(\tau-\alpha_1)e^{-\alpha_1 T}]}{(E+\beta^4)(\alpha_2-\alpha_1)}\right] J_o(\beta R)\,\beta\, d\beta \tag{78}$$

For the stresses, the "s" factor of equations 41 becomes, with the use of partial fractions,

$$\frac{1}{s}\,\frac{\overline{D}_T}{1+\overline{D}_T\beta^4} = \frac{1}{(E+\beta^4)(\alpha_2-\alpha_1)}\left[\frac{(\tau-\alpha_1)}{(s+\alpha_1)} - \frac{(\tau-\alpha_1)}{(s+\alpha_2)}\right] \tag{79}$$

Taking the inverse Laplace transform of equations 41 we get

$$\frac{(\sigma_\theta+\sigma_r)h^2}{2PC(1+\nu)} = \frac{3H(T)}{2\pi}\int_0^\infty \frac{J_1(\beta A)}{\beta A/2}\; J_o(\beta R)\left[\frac{(\tau-\alpha_1)e^{-\alpha_1 T}-(\tau-\alpha_2)e^{-\alpha_2 T}}{(E+\beta^4)(\alpha_2-\alpha_1)}\right]\beta^3\, d\beta\,, \tag{80a}$$

$$\frac{(\sigma_\theta-\sigma_r)h^2}{2PC(1-\nu)} = \frac{3H(T)}{2\pi}\int_0^\infty \frac{J_1(\beta A)}{\beta A/2}\;\frac{J_1(\beta R)}{\beta R/2}\left[\frac{(\tau-\alpha_1)e^{-\alpha_1 T}-(\tau-\alpha_2)e^{-\alpha_2 T}}{(E+\beta^4)(\alpha_2-\alpha_1)}\right]\beta^3\, d\beta \tag{80b}$$

$$- \frac{(\sigma_\theta+\sigma_r)h^2}{2PC(1+\nu)} \,.$$

When β goes to infinity the same type singularities exist for equations 78 and 80 as existed for equations 31 and 43 in secondary creep. Hence, for equations 80 we must subtract the T=0 part to make the integrals converge when both R=0 and A=0.

For A=0 we could investigate the deflection and stresses as a function of R, but nothing really new is expected. At T=0 one would expect the deflections to be less than those shown on Figure 9 at T=0. As T increases the deflection profile should approach those in Figure 9. At T=0 one would expect the stresses to be greater than the ones shown in Figures 10 and 11. As T increases these stress profiles should approach those of Figures 10 and 11. When R=0 and A is small, we would again expect to find very little influence of A in the asterisked deflections and stresses.

Let us now proceed to the more important case of A=0 and R=0. As before we transform the integrals according to the exponent of the exponential functions. That is, we let $x = \alpha_1 T$ for one part of the integral, and $y = \alpha_2 T$ for the other part. Since this transformation is more complicated than the case for secondary creep, some of the important steps of the transformation are outlined as follows.

From equation 77, we find that α_1 and α_2 are the roots of

$$(E+\beta^4)\alpha^2 - (1+\tau+\tau\beta^4)\alpha + \tau = 0 \ , \tag{81a}$$

and defining λ_1 and λ_2 as the values of α_1 and α_2 when $\beta=0$, λ_1 and λ_2 must be the roots of

$$E\lambda^2 - (1+\tau)\lambda+\tau=0. \tag{81b}$$

Solving equation 81a for β^4, and using the factored form of equation 81b, we obtain

$$\beta^4 = \frac{E\alpha^2-(1+\tau)\alpha+\tau}{\alpha(\tau-\alpha)} = \frac{E(\alpha-\lambda_1)(\alpha-\lambda_2)}{\alpha\ (\tau-\alpha)} . \tag{82a}$$

This equation, which shows how α_1 and α_2 depend on β^4, is shown in Figure 13. Solving equation 81b for τ, we obtain

$$\tau = \frac{\lambda(1-E\lambda)}{1-\lambda} . \tag{82b}$$

This equation, which shows how λ_1 and λ_2 depend on τ and E, is shown in Figure 14. Two other useful relations are

$$\lambda_1 + \lambda_2 = \frac{(1+\tau)}{E} \tag{83a}$$

and

$$\lambda_1 \lambda_2 = \tau/E . \tag{83b}$$

The above transformations are due to S. Takagi [66]. In order to transform equations 78 and 80 for R=0 and A=0, we must substitute equation 82a. The algebra is a little tedious but straightforward. For example, differentiating equation 82a we get

$$4\beta^3 d\beta = \left[\frac{E\tau-1-\tau}{(\tau-\alpha)^2} - \frac{1}{\alpha^2}\right] d\alpha \tag{84}$$

where α can be either α_1 or α_2 depending upon which part of the integral we are dealing with. Grinding through the algebra for equation 80a we get

$$\frac{(\sigma_\theta+\sigma_r)^* h^2}{2PC(1+\nu)} = - \frac{3H(T)}{8\pi} \left[\int_0^{\lambda_1 T} \frac{1-e^{-x}}{x} dx + \int_{\tau T}^{\lambda_2 T} \frac{1-e^{-y}}{y} dy\right], \tag{85}$$

which integrates to

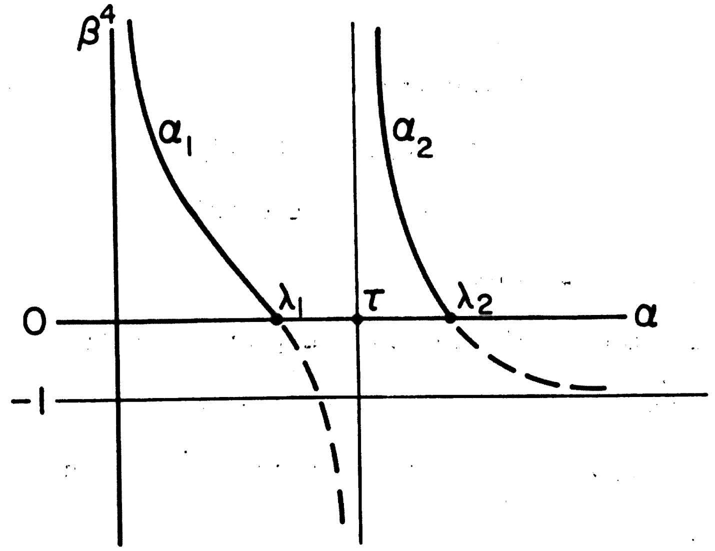

Figure 13. α_1 and α_2 as a function of β^4 for primary creep.

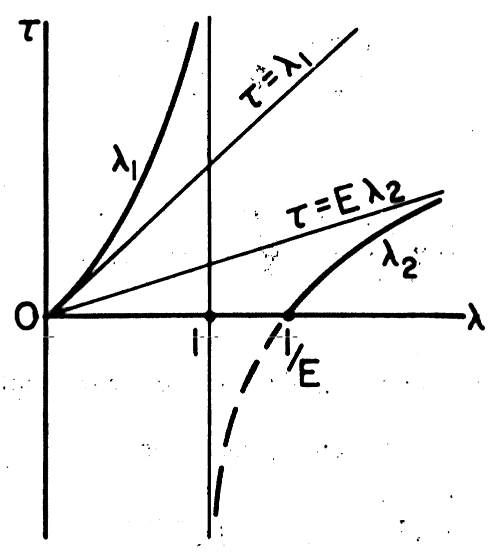

Figure 14. λ_1 and λ_2 as a function of E and τ for primary creep.

$$\frac{(\sigma_\theta+\sigma_r)^* h^2}{2PC(1+\nu)} = -\frac{3H(T)}{8\pi}\,[E_1(\lambda_1 T) + E_1(\lambda_2 T) - E_1(\tau T) + \gamma + \log(T/E)] \quad (86)$$

In equations 85 and 86 the T=0 solution has been subtracted. For primary creep, the T=0 solution is just the elastic solution using ℓ defined with E_1, rather than with E_o. To obtain the actual stress we must add this elastic solution.

In order to compare the primary creep stress with the secondary creep stress of equation 63b, we must also subtract the elastic solution using ℓ defined with E_o. From equation 59, we find that the sum of the two corrections is

$$-\frac{3}{8\pi}\log E\ ,$$

which should be added to equation 86 to make the comparison.

Transforming equation 78 with A=0 and R=0 we get

$$\frac{wk\ell^2}{PH(T)} = \frac{\sqrt{E}}{8} + \frac{\sqrt{E}}{8\pi}\int_o^{\lambda_1 T} \frac{1-e^{-x}}{x}\sqrt{\frac{\lambda_1 T-x}{x}}\sqrt{\frac{\lambda_2 T-x}{\tau T-x}}\,dx$$

$$+\frac{\sqrt{E}}{8\pi}\int_{\tau T}^{\lambda_2 T} \frac{1-e^{-y}}{y}\sqrt{\frac{y-\lambda_1 T}{y}}\sqrt{\frac{\lambda_2 T-y}{y-\tau T}}\,dy\ . \quad (87)$$

The elastic part, $\sqrt{E}/8$, of equation 87 has not been subtracted. Letting $x=\lambda_1 Tz$ and $y=\lambda_2 T-(\lambda_2-\tau)Tz$, equation 87 becomes

$$\frac{wk\ell^2}{PH(T)} = \frac{\sqrt{E}}{8} + \frac{1}{8\pi\sqrt{\lambda_1}}\int_o^1 \frac{1-e^{-\lambda_1 Tz}}{z}\sqrt{\frac{1-z}{z}}\sqrt{\frac{1-z\lambda_1/\lambda_2}{1-z\lambda_1/\tau}}\,dz$$

$$+\frac{\sqrt{E}}{8\pi}(\lambda_2-\tau)\int_o^1 \left[1-e^{-\lambda_2 T+(\lambda_2-\tau)Tz}\right]\sqrt{\frac{z}{1-z}}\sqrt{\frac{\lambda_2-\lambda_1-z(\lambda_2-\tau)}{[\lambda_2-z(\lambda_2-\tau)]^3}}\,dz. \quad (89)$$

Expanding the last factor in each integrand into a power series in z, we can integrate to obtain

$$\frac{wk\ell^2}{PH(T)} = \frac{\sqrt{E}}{8} + \frac{1}{8\sqrt{\lambda_1}} \sum_{n=0}^{\infty} \frac{a_n (2n-3)!!}{2^n\ n!} \left[1 - {}_1F_1(n-.5,\ n+1,\ -\lambda_1 T)\right]$$

$$+ \frac{\sqrt{E}}{8} \sqrt{\frac{\lambda_2-\lambda_1}{\lambda_2}}\ \frac{\lambda_2-\tau}{\lambda_2} \sum_{n=0}^{\infty} \frac{b_n}{2^{n+1}} \frac{(2n+1)!!}{(n+1)!} \left[1-e^{-\tau T}\ {}_1F_1(\tfrac{1}{2},n+2;-(\lambda_2-\tau)T)\right],$$

where ${}_1F_1$ is the confluent hypergeometric function,

$$a_n = -\left(\frac{\lambda_1}{2\tau}\right)^n \sum_{p=0}^{n} \frac{(2p-3)!!}{p!} \frac{(2n-2p-1)!!}{(n-p)!} \left(\frac{\tau}{\lambda_2}\right)^p, \tag{90a}$$

and

$$b_n = -\left(\frac{\lambda_1-\tau}{\lambda_2-\lambda_1}\right)^n \frac{1}{2^n} \sum_{p=0}^{n} \frac{(2p+1)!!}{p!} \frac{(2n-2p-3)!!}{(n-p)!} \left(\frac{\lambda_2-\lambda_1}{\lambda_2}\right)^p. \tag{90b}$$

In these formulas $(n)!! = 1\cdot3\cdot5\cdots n$. By definition $(-1)!! = 1$ and $(-3)!!=-1$.

Equation 86 and 89 can be easily evaluated, but before doing this, let us develop the tertiary creep solution so that a comparison can be made.

TERTIARY CREEP

For tertiary creep equation 8 reduces to

$$\frac{1}{2G} = \frac{1}{E_o} + \frac{1}{\eta_1 \partial/\partial t} + \frac{1}{-E_3+\eta_3 \partial/\partial t} . \tag{91}$$

We let $2G=E_o\ D_T$ with $T = E_o t/\eta_o$ as before, but now

$$D_T = \frac{\partial/\partial T\ (-\xi+\partial/\partial T)}{\partial^2/\partial T^2+(1-\xi)\partial/\partial T - \xi\eta} , \tag{92}$$

where

$$\xi = (\eta_o E_3)/(E_o \eta_3) \tag{93a}$$

and

$$\eta = \eta_o/\eta_1 . \tag{93b}$$

Note that $0 \leqslant \xi \leqslant \infty$ and $0 \leqslant \eta \leqslant 1$. We proceed exactly as we did for secondary creep, except now

$$\bar{D}_T = \frac{s(s-\xi)}{s^2+s(1-\xi)-\xi\eta} . \tag{94}$$

The "s" factor in equation 27 now becomes, with the use of partial fractions,

$$\frac{1}{s(1+\bar{D}_T\beta^4)} = \frac{1}{s} + \frac{\beta^4}{(1+\beta^4)(\alpha_4-\alpha_3)}\left[\frac{\xi+\alpha_3}{s+\alpha_3} - \frac{\xi+\alpha_4}{s+\alpha_4}\right], \tag{95}$$

where

$$\alpha_3 = \frac{(1-\xi-\xi\beta^4) - [(1-\xi-\xi\beta^4)^2 + 4\xi\eta(1+\beta^4)]^{\frac{1}{2}}}{2(1+\beta^4)} \tag{96a}$$

$$\alpha_4 = \frac{(1-\xi-\xi\beta^4) + [(1-\xi-\xi\beta^4)^2 + 4\xi\eta(1+\beta^4)]^{\frac{1}{2}}}{2(1+\beta^4)} . \qquad (96b)$$

We note that α_3 and α_4 are the negative roots of

$$s^2(1+\beta^4) + s(1-\xi-\xi\beta^4) - \xi\eta = 0 . \qquad (97)$$

Using equation 18b, the inverse Laplace transform of equation 27 becomes

$$\frac{wk\ell^2}{P} = \frac{H(T)}{2\pi} \int_0^\infty \frac{J_1(\beta A)}{\beta A/2} \left[1+ \frac{\beta^4[(\xi+\alpha_3)e^{-\alpha_3 T} - (\xi+\alpha_4)e^{-\alpha_4 T}]}{(1+\beta^4)(\alpha_4-\alpha_3)}\right] J_o(\beta R)\ \beta d\beta \qquad (98)$$

For the stresses the "s" factor in equation 41 becomes, with the use of partial fractions,

$$\frac{\overline{D}_T}{s(1+\overline{D}_T\beta^4)} = \frac{1}{(1+\beta^4)(\alpha_4-\alpha_3)} \left[- \frac{(\xi+\alpha_3)}{s+\alpha_3} + \frac{(\xi+\alpha_4)}{s+\alpha_4}\right] . \qquad (99)$$

Taking the inverse Laplace transform of equation 41 we get

$$\frac{(\sigma_\theta+\sigma_r)h^2}{2PC(1+\nu)} = \frac{3H(T)}{2\pi} \int_0^\infty \frac{J_1(\beta A)}{\beta A/2} \left[\frac{-(\xi+\alpha_3)e^{-\alpha_3 T} + (\xi+\alpha_4)e^{-\alpha_4 T}}{(1+\beta^4)(\alpha_4-\alpha_3)}\right] J_o(\beta R)\beta^3 d\beta \qquad (100a)$$

$$\frac{(\sigma_\theta-\sigma_r)h^2}{2PC(1-\nu)} = \frac{3H(T)}{2\pi} \int_0^\infty \frac{J_1(\beta A)}{\beta A/2} \left[\frac{-(\xi+\alpha_3)e^{-\alpha_3 T} + (\xi+\alpha_4)e^{-\alpha_4 T}}{(1+\beta^4)(\alpha_4-\alpha_3)}\right] \frac{J_1(\beta R)}{\beta R/2}\ \beta^3 d\beta$$

$$- \frac{(\sigma_\theta+\sigma_r)h^2}{2PC(1+\nu)} . \qquad (100b)$$

When β goes to infinity, the same type singularities exist for equations 98 and 100 as existed for equations 31 and 43 in secondary creep. Hence, for equations 100 we must subtract the T=0 part to make the integrals converge when both R=0 and A=0. The T=0 part for tertiary creep is the same as for secondary creep.

For A=0 we would expect the same results as shown in Figures 9, 10, and 11 for small T. For large T one would expect to have a greater deflection and a lesser stress. When R=0 and A is small, we would again expect to find very little influence on the asterisked deflection and stresses.

Let us now proceed to the more important case of A=0 and R=0. This proceeds in a way that is similar to the transformation for primary creep, but this time we let $x = \alpha_3 T$ and $y = \alpha_4 T$.

We note that α_3 and α_4 are roots of the equation

$$(1+\beta^4)\,\alpha^2 - (1-\xi-\xi\beta^4)\,\alpha - \xi\eta = 0. \tag{101a}$$

Defining λ_3 and λ_4 as the values of α_3 and α_4 when $\beta=0$, λ_3 and λ_4 must be the roots of

$$\lambda^2 - (1-\xi)\lambda - \xi\eta=0 . \tag{101b}$$

Solving equation 101a for β^4 and using the factored form of equation 101b, we obtain

$$\beta^4 = -\frac{(\alpha-\lambda_3)(\alpha-\lambda_4)}{\alpha(\alpha+\xi)} . \tag{102a}$$

This equation which shows how α_3 and α_4 depend upon β^4 is shown in Figure 15. Solving equation 101b for ξ we obtain

$$\xi = \frac{\lambda(1-\lambda)}{(\lambda-\eta)} . \tag{102b}$$

This equation, which shows how λ_3 and λ_4 depend on ξ and η, is shown in Figure 16. Two other useful relations are

$$\lambda_3 + \lambda_4 = 1-\xi \tag{103a}$$

and

$$\lambda_3 \lambda_4 = -\xi\eta . \tag{103b}$$

For R=0 and A=0, we change the variable of integration in equation 100a to obtain

$$\frac{(\sigma_\theta+\sigma_r)^* h^2}{2PC(1+\nu)} = - \frac{3H(T)}{8\pi} \left[\int_0^{\lambda_4 t} \frac{1-e^{-y}}{y} \, dy - \int_{\lambda_3 T}^{-\xi T} \frac{1-e^{-x}}{x} \, dx \right], \tag{104}$$

where the T=0 part has been subtracted. This is written as

$$\frac{(\sigma_\theta+\sigma_r)^* h^2}{2PC(1+\nu)} = - \frac{3H(T)}{8\pi} \quad [E_1(\lambda_4 T) + E_i(\xi T) - E_i(-\lambda_3 T) + \log (\eta T) + \gamma], \tag{105}$$

where $E_i(z)$ is another type of exponential integral. Its series expansion is

$$E_i(z) = \sum_{n=1}^{\infty} \frac{z^n}{n \, n!} + \log z + \gamma . \tag{106a}$$

For large z we again develop a simple formula for $E_i(z)$ which is

$$E_i(z) \simeq \frac{e^z}{z} \; \frac{z+0.081}{z-1.163} . \tag{106b}$$

This formula has less than 3% error when z is greater than 4. The two constants were determined by passing the equation through the points z=4 and z=8.

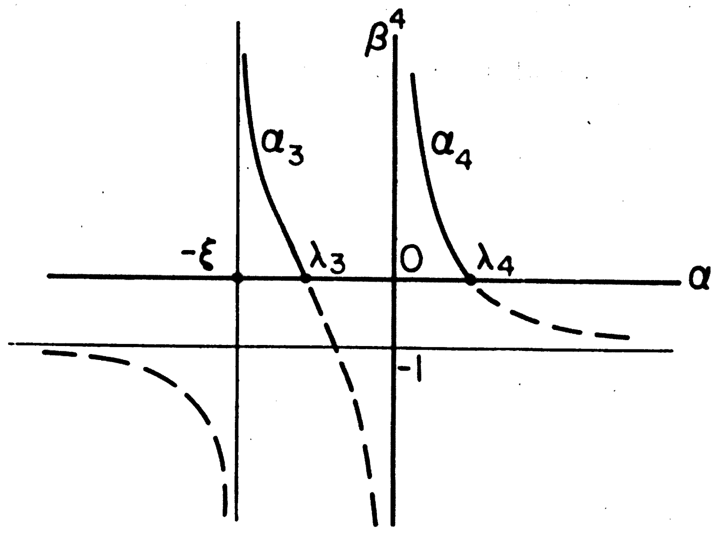

Figure 15. α_3 and α_4 as a function of β^4 for tertiary creep.

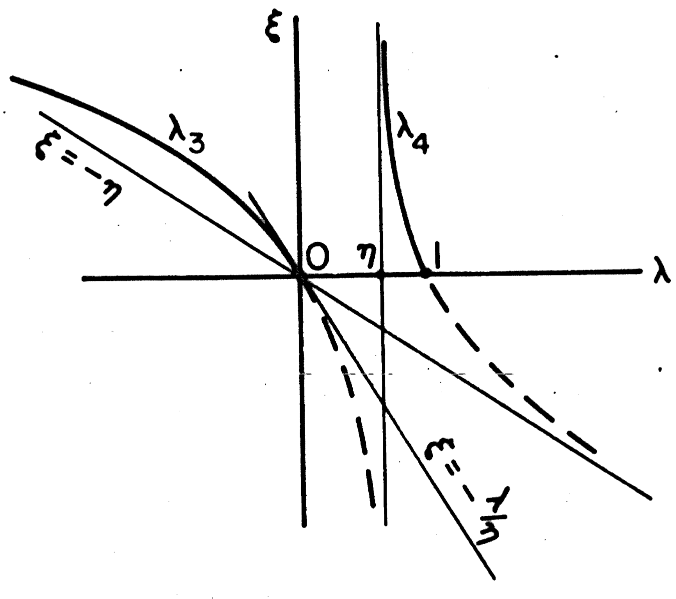

Figure 16. λ_3 and λ_4 as a function of η and ξ for tertiary creep.

For R=0 and A=0 equation 98 with the change of the integration variable becomes

$$\frac{wk\ell^2}{PH(T)} = \frac{1}{8} + \frac{1}{8\pi}\int_o^{\lambda_4 T} \frac{1-e^{-y}}{y} \sqrt{\frac{\lambda_4 T-y}{y}} \sqrt{\frac{y-\lambda_3 T}{y+\xi T}}\, dy$$

$$- \frac{1}{8\pi}\int_{\lambda_3 T}^{-\xi T} \frac{1-e^{-x}}{x} \sqrt{\frac{\lambda_3 T-x}{x+\xi T}} \sqrt{\frac{\lambda_4 T-x}{-x}}\, dx \,. \tag{107}$$

Letting $y = \lambda_4 T(1-z)$ and $x = -\xi T+(\xi+\lambda_3)Tz$, equation 107 becomes

$$\frac{wk\ell^2}{PH(T)} = \frac{1}{8} + \frac{1}{8\pi}\int_o^1 \frac{1-e^{-\lambda_4 T(1-z)}}{1-z} \sqrt{\frac{z}{1-z}} \sqrt{\frac{\lambda_4-\lambda_3}{\lambda_4+\xi}} \sqrt{\frac{1-\lambda_4 z\,/\,(\lambda_4-\lambda_3)}{1-\lambda_4 z/\,(\lambda_4+\xi)}}\, dz$$

$$- \frac{1}{8\pi}\frac{(\xi+\lambda_3)}{\xi}\int_o^1 \frac{1-e^{\xi T-(\xi+\lambda_3)Tz}}{} \sqrt{\frac{1-z}{z}} \sqrt{\frac{\lambda_4+\xi}{\xi}} \sqrt{\frac{1-(\xi+\lambda_3)z/(\xi+\lambda_4)}{[1-(\xi+\lambda_3)z/\xi]^3}}\, dz \,. \tag{108}$$

Expanding the last factor in each integrand into a power series in z and integrating, one obtains

$$\frac{wk\ell^2}{PH(T)} = \frac{1}{8} + \frac{1}{8}\sqrt{\frac{\lambda_4-\lambda_3}{\lambda_4+\xi}} \sum_{n=0}^{\infty} a_n \frac{(2n+1)!!}{n!2^n} [-1 + {}_1F_1(-.5,\, n+1;\, -\lambda_4 T)]$$

$$- \frac{1}{8}\frac{\xi+\lambda_3}{\xi}\sqrt{\frac{\lambda_4+\xi}{\xi}} \sum_{n=0}^{\infty} b_n \frac{(2n-1)!!}{(n+1)!\,2^{n+1}} \left\{1-e^{\xi T}\, {}_1F_1\left[n+\tfrac{1}{2},\, n+2; -(\xi+\lambda_3)T\right]\right\}, \tag{109}$$

where

$$a_n = -\left(\frac{\lambda_4}{\lambda_4-\lambda_3}\right)^n \frac{1}{2^n} \sum_{p=0}^{n} \frac{(2n-2p-3)!!}{(n-p)!} \frac{(2p-1)!!}{p!} \left(\frac{\lambda_4-\lambda_3}{\lambda_4+\xi}\right)^p \tag{110a}$$

and

$$b_n = -\left(\frac{\xi+\lambda_3}{\xi}\right)^n \frac{1}{2^n} \sum_{p=o}^{n} \frac{(2p-3)!!}{p!} \frac{(2n-2p+1)!!}{(n-p)!} \left(\frac{\xi}{\xi+\lambda_4}\right)^p \,. \tag{110b}$$

COMPARISON AND APPLICATION

Let us now compare the results of the deflection and stress when R=0 and A=0. The deflections "w" for primary, secondary, and tertiary creep are given by equations 89, 63a, and 109 respectively. The stresses $(\sigma_\theta+\sigma_r)^*$ for primary, secondary, and tertiary creep are given by equations 86, 63b, and 105 respectively. Recall that $(-3/8\pi)\log E$ must be added to equation 86 in order to make these comparison.

For secondary creep the material constant E_o enters the solution through the flexural rigidity length "ℓ", which has been used to make the lengths "r" and "a" dimensionless. The material constant η_o enters the ratio η_o/E_o, which has been used to make the time dimensionless. Since all the material constants for secondary creep are absorbed in this manner, it is possible to perform numerical computations without specifying E_o and η_o.

However, the same is not true for primary and tertiary creep. In primary creep the additional material constants E_2 and η_2 enter the solution through the parameters $E = E_o/E_1$ and $\tau = (\eta_o E_2)/(\eta_2 E_o)$, which are dimensionless. In tertiary creep the additional material constants E_3 and η_3 enter the solution through the parameters $\eta=\eta_o/\eta_1$ and $\xi=(\eta_o E_3)/(\eta_3 E_o)$, which are dimensionless. These parameters must be specified in order to perform numerical computations.

Since the parameters for primary and tertiary creep are not well determined, we will make a comparison with E=0.25, τ=1, η=0.8, and ξ=0.2, which have been arbitrarily selected. The comparison of the deflections as a function of time is given in Figure 17. This is the first time that accelerating creep for a floating ice sheet has been predicted. In general, the deflection increases as time increases.

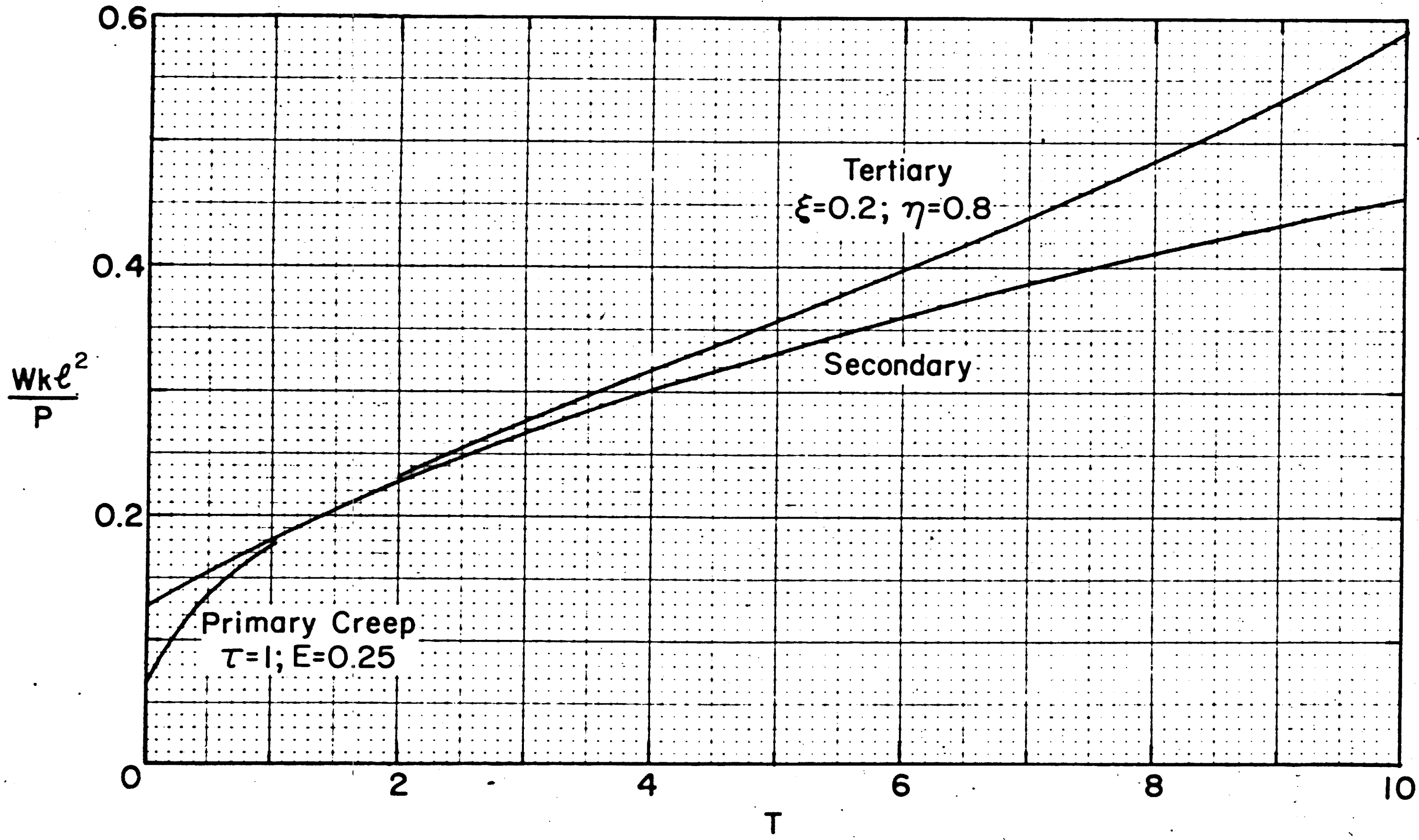

Figure 17. The comparison of deflections under a concentrated load as a function of time.

The comparison of the stresses as a function of time is shown in Figure 18. In general, the stresses decrease as a function of time; i.e., stress relaxation occurs. The results are tabulated in Table 6 for secondary creep. Since the material constants for primary and tertiary creep are only illustrative, these results are not tabulated.

If a maximum tensile stress is used as a failure criterion, then the results of Figure 18 would indicate that the ice should crack immediately or not at all. But as mentioned earlier, the ice has been known to crack sometime after the load has been applied. An explanation for this is that the tensile strength of the ice may decrease with time due to the creep process within the ice. John Burdick [67] has performed some tensile tests for strength under creep which indicate that this is true at first. But for creep tests lasting a long time, Burdick's tensile strength was as much as twice the instantaneous tensile strength.

In order to help select reasonable material constants, let us now discuss creep tests which have been performed on floating ice sheets. D.F. Panfilov [68] has conducted creep tests lasting for a duration of 6 hours on floating ice sheets which were up to 5.6 cm thick. The principal purpose of these tests was to determine the bearing capacity load as a function of time. In these tests, the ice sheet became flooded in the deflected area because a small hole was placed through the ice sheet. This water on top of the ice provided an additional load compared to the problem solved in this paper. Panfilov shows that the deflection increases linearly with time. He gives no values for the material constants.

G.E. Frankenstein [32] has reported on bearing capacity tests which were conducted on lake ice from 6 to 18 inches thick. Since the

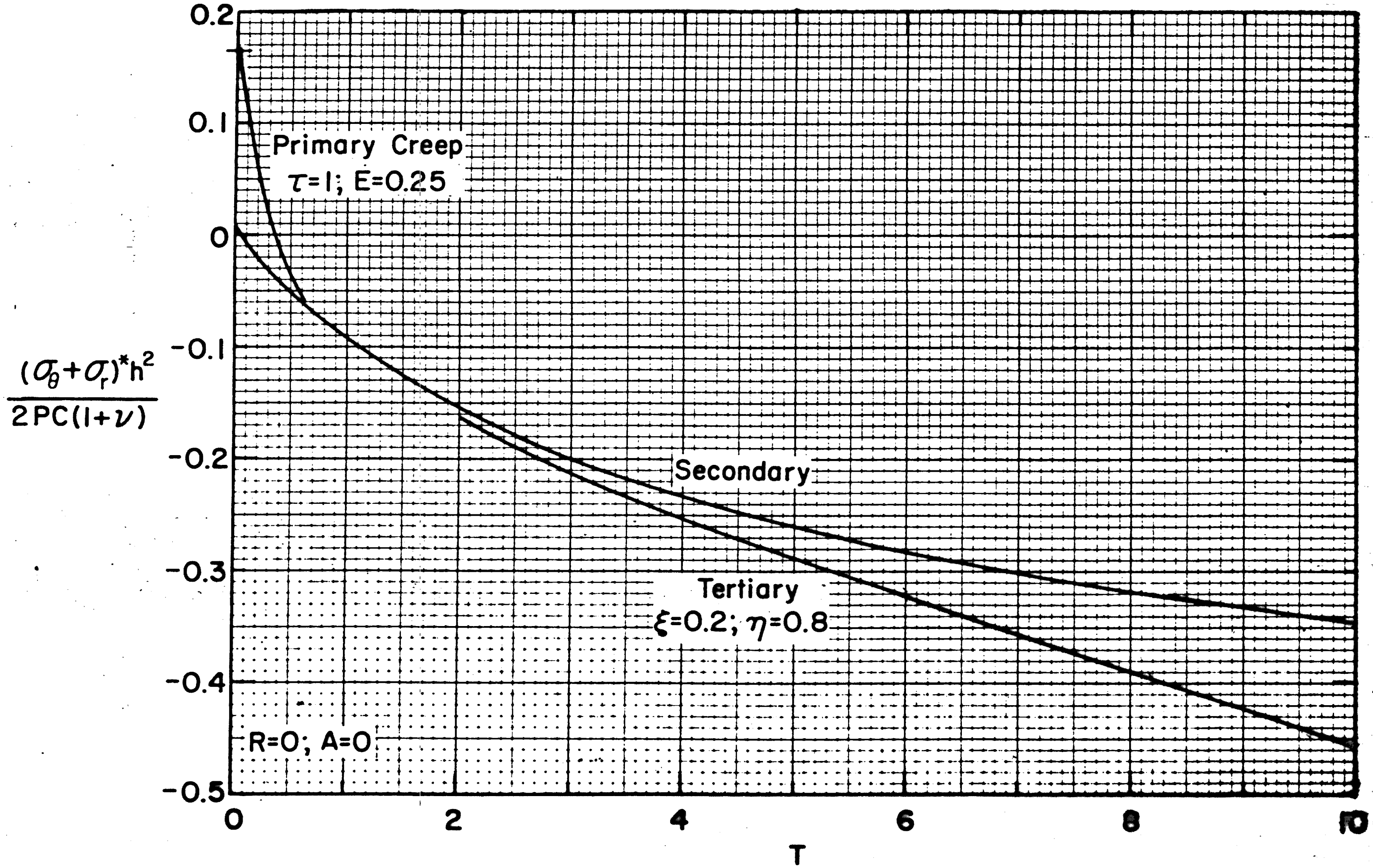

Figure 18. The comparison of stresses $(\sigma_\theta+\sigma_r)^*$ under a concentrated load as a function of time.

Table 6. Secondary Creep When R=0 and A=0

T	$\frac{wk\ell^2}{P}$	$\frac{(\sigma_\theta+\sigma_r)^* h^2}{2PC(1+\nu)}$
0	.125 000	0.0
.1	.131 173	-.011 645
.2	.137 198	-.022 731
.3	.143 080	-.033 294
.4	.148 828	-.043 366
.5	.154 448	-.052 980
.6	.159 944	-.062 162
.7	.165 324	-.070 940
.8	.170 592	-.079 339
.9	.175 753	-.087 381
1.0	.176 028	-.095 087
1.1	.185 772	-.102 477
1.2	.190 640	-.109 571
1.3	.195 417	-.116 385
1.4	.200 109	-.122 936
1.5	.204 718	-.129 238
1.6	.209 248	-.135 305
1.7	.213 702	-.141 151
1.8	.218 083	-.146 787
1.9	.222 394	-.152 225
2.0	.226 637	-.157 476
2.1	.230 816	-.162 549
2.2	.234 932	-.167 455
2.3	.238 988	-.172 261
2.4	.242 984	-.176 796
2.5	.246 926	-.181 248
2.6	.250 813	-.185 564
2.7	.254 648	-.189 750
2.8	.258 432	-.193 814
2.9	.262 168	-.205 241
3.0	.265 857	-.201 595
3.1	.269 499	-.205 323
3.2	.273 098	-.208 950
3.3	.276 654	-.212 481
3.4	.280 169	-.215 919
3.5	.283 643	-.219 270
3.6	.287 078	-.222 536
3.7	.290 476	-.225 721
3.8	.293 837	-.228 829
3.9	.297 162	-.231 864
4.0	.300 452	-.234 828
4.1	.303 709	-.237 724
4.2	.306 934	-.240 555
4.3	.310 126	-.243 324
4.4	.313 287	-.246 032
4.5	.316 419	-.251 279
4.6	.319 521	-.251 279
4.7	.322 594	-.253 822
4.8	.325 640	-.256 313
4.9	.328 658	-.258 755

T	$\frac{wk\ell^2}{P}$	$\frac{(\sigma_\theta+\sigma_r)^* h^2}{2PC(1+\nu)}$
5.0	.331 650	-.261 150
5.1	.334 616	-.263 498
5.2	.337 557	-.265 803
5.3	.340 474	-.268 064
5.4	.343 366	-.270 285
5.5	.346 235	-.272 466
5.6	.349 081	-.274 608
5.7	.351 904	-.276 714
5.8	.354 706	-.278 783
5.9	.357 486	-.280 818
6.0	.360 245	-.282 819
6.1	.362 984	-.284 787
6.2	.365 703	-.286 724
6.3	.368 402	-.288 630
6.4	.371 082	-.290 507
6.5	.373 743	-.292 354
6.6	.376 385	-.294 174
6.7	.379 009	-.295 967
6.8	.381 616	-.297 733
6.9	.384 205	-.299 474
7.0	.386 777	-.301 190
7.1	.389 333	-.302 881
7.2	.391 872	-.304 550
7.3	.394 395	-.306 195
7.4	.396 902	-.307 818
7.5	.399 394	-.309 419
7.6	.401 870	-.310 999
7.7	.404 331	-.312 559
7.8	.406 778	-.314 099
7.9	.409 210	-.315 619
8.0	.411 628	-.317 120
8.1	.414 032	-.318 602
8.2	.416 472	-.320 066
8.3	.418 799	-.321 513
8.4	.421 163	-.322 942
8.5	.423 513	-.324 354
8.6	.425 851	-.325 750
8.7	.428 176	-.327 130
8.8	.430 488	-.328 494
8.9	.432 788	-.329 842
9.0	.435 077	-.331 176
9.1	.437 353	-.332 495
9.2	.439 617	-.333 799
9.3	.441 871	-.335 089
9.4	.444 112	-.336 366
9.5	.446 343	-.337 629
9.6	.448 563	-.338 879
9.7	.450 771	-.340 116
9.8	.452 969	-.341 340
9.9	.455 157	-.342 552
10.0	.457 334	-.343 751

purpose of these tests was to determine bearing capacity, the tests were of short duration with the length varying from 9 to 31 minutes. The ice sheet was loaded by pumping water at a constant rate into a tank resting on the ice sheet. The deflection profile was measured and analyzed assuming a secondary creep model as shown in Figure 7a. Frankenstein obtained values of E_o ranging from 5,000 to 30,000 kgf/cm^2, and values of η_o/E_o ranging from 1 to 4 minutes. It should be pointed out that since the tests were of short duration, secondary creep may not have been reached. Furthermore, since heavy loads were used to obtain breakthrough, radial and circumferential cracks developed during the tests. These cracks caused an additional deflection of the ice sheet.

Marlin Sundberg-Falkenmark [69] has performed creep tests as well as breakthrough tests on lake ice. The creep tests were on ice from 37 to 50 cm thick and up to 156 minutes long. The deflection profiles were not tabulated but presented in graphical form. These profiles were analyzed using elastic theories rather than a time-dependent theory. Hence, even though these creep tests have been conducted, the details have not presented in a manner that allows us to obtain the material constants for our model.

A.E. IAkunin [51] has reported a summary of creep tests performed on fresh water ice. In a model basin with ice from 3 to 10 cm thick, ten creep tests were conducted with the length of the tests varying from 1 to 5.5 hours. On lake ice from 13 to 94 cm thick, twenty-two creep tests were conducted with the maximum length of any test being 235 hours. During some of these tests, cracking and flooding of the ice sheet occurred. IAkunin analyzed his data according to the primary creep model of Figure 6a. He reported only average values of $E_2/E_1=0.2$ and $\eta_2/\eta_o=0.05$ for the material constants. These values correspond to $E=E_o/E_1=1/6$ and $\tau=(\eta_o E_2)/\eta_2 E_o)=24$, and appear to be the best estimate for the primary creep properties. Using these values, the deflection and the asterisked stress are tabulated in Table 7. Figure 19 and 20 show these results in graphical from.

Estimates of E_1 can be made from elastic data. The uniaxial test data presented by Hawkes and Mellor [70] give an average value of Young's modulus of 63,000 kgf/cm^2. Assuming a Poisson's ratio of 0.5, our estimate of E_1 is 63,000/(1+ν) or 42,000 kgf/cm^2. Using IAkunin's value of $E_o/E_1=1/6$, we obtain E_o=7,000 kgf/cm^2. This value falls in the low end of the range of Frankenstein's data.

An estimate for η_o/E_o is more difficult to make since the data from uniaxial tests show a wide scatter. Mellor and Testa [71] report an average viscosity of 0.13 x 10^{10} kgf/cm^2-sec. Dividing by (1+ν) with ν=0.5 and using E_o=7,000 kgf/cm^2, we get η_o/E_o=34 hours. If this estimate is correct, then from Figures 19 and 20 we see that the primary creep has been completed in about 3.4 hours.

The only published creep tests on floating sea ice are those of Hobbs and Kingery [72]. They made no analysis of the data. Vaudrey and Katona [56] have performed uniaxial compression tests on sea ice, and have expressed their results with a model that has a spring in series with two delayed elasticity elements. They assumed ν=0.3 and obtained values for the model representing 2G as E_1=9500 kgf/cm^2, E_2=1400 kgf/cm^2, η_2/E_2=6.7 hours, E_3=8200 kgf/cm^2, and η_3/E_3=4.2 minutes. Our E_o would be defined by $1/E_o = 1/E_1 + 1/E_2 + 1/E_3$ which gives a value of E_o = 1000 kgf/cm^2. Using these values in their finite element program they obtained reasonable agreement with the data of Hobbs and Kingery. However, Vaudrey and Katona point out that they did not choose the material constants by curve fitting to the field data.

Let us now consider an example of the procedure for estimating the stress under a load on an ice sheet. Assuming A=0 one can calculate the stress $(\sigma_\theta+\sigma_r)^* h^2/[2PC(1+\nu)]$ as a function of time T from either equation 86, 63b, or 105. The choice among these equations depends on whether the time T is in primary, secondary, or tertiary creep respectively. To this stress we must add the elastic stress $(\sigma_\theta+\sigma_r)^o h^2/[2PC(1+\nu)]$ from equation 57 with A≠0, in order to obtain the total stress $(\sigma_\theta+\sigma_r)h^2/[2PC(1+\nu)]$. If a second load is on the ice sheet in the vicinity of the first load, the stress produced by the second load at the location of the first load must be added. In this case with A=0, the values of $(\sigma_\theta+\sigma_r)^* h^2/[2PC(1+\nu)]$ and $(\sigma_\theta-\sigma_r)^* h^2/[2PC(1-\nu)]$ as a function of R and T can be obtained by numerical integration by the method given in this paper. To this stress must be added the elastic parts with A≠0 as given in equation 47a and 47b.

Table 7. Primary Creep for τ=24 and E=1/6 When R=0 and A=0

T	$\frac{wk\ell^2}{P}$	$\frac{(\sigma_\theta+\sigma_r)^* h^2}{2PC(1+\nu)}$
0	.051 031	.213 875
.001	.054 155	.199 460
.002	.057 122	.186 212
.003	.059 938	.174 022
.004	.062 613	.162 789
.005	.065 155	.152 425
.006	.067 575	.142 850
.007	.069 878	.133 992
.008	.072 075	.125 786
.009	.074 171	.118 173
.010	.076 171	.111 102
.011	.078 082	.104 527
.012	.079 909	.098 404
.013	.081 657	.092 696
.014	.083 331	.087 368
.015	.084 934	.082 388
.016	.086 471	.077 728
.017	.087 945	.073 363
.018	.089 361	.069 268
.019	.090 720	.065 424
.020	.092 025	.061 810
.021	.093 281	.058 410
.022	.094 488	.055 206
.023	.095 650	.052 186
.024	.096 769	.049 334
.025	.097 846	.046 640
.026	.098 885	.044 092
.027	.099 886	.041 680
.028	.100 851	.039 394
.029	.101 783	.037 227
.030	.102 683	.035 169
.031	.103 551	.033 215
.032	.104 390	.031 356
.033	.105 201	.029 588
.034	.105 985	.027 904
.035	.106 742	.026 298
.036	.107 476	.024 768
.037	.108 185	.023 306
.038	.108 872	.021 911
.039	.109 537	.020 577
.040	.110 182	.019 301
.041	.110 807	.018 079
.042	.111 412	.016 910
.043	.111 998	.015 788
.044	.112 567	.014 713
.045	.113 119	.013 682
.046	.113 654	.012 682
.047	.114 174	.011 740
.048	.114 679	.010 826
.049	.115 169	.009 946

Table 7 (con't)

T	$\frac{wk\ell^2}{P}$	$\frac{(\sigma_\theta+\sigma_r)^* h^2}{2PC(1+\nu)}$
.050	.115 644	.009 100
.051	.116 107	.008 285
.052	.116 556	.007 501
.053	.116 993	.006 744
.054	.117 418	.006 015
.055	.117 831	.005 311
.056	.118 233	.004 631
.057	.118 624	.003 975
.058	.119 006	.003 341
.059	.119 377	.002 728
.060	.119 738	.002 136
.061	.120 089	.001 562
.062	.120 432	.001 007
.063	.120 765	.000 469
.064	.121 091	-.000 053
.065	.121 408	-.000 558
.066	.121 717	-.001 048
.067	.122 019	-.001 523
.068	.122 313	-.001 985
.069	.122 600	-.002 433
.070	.122 880	-.002 868
.071	.123 154	-.003 292
.072	.123 421	-.003 703
.073	.123 682	-.004 104
.074	.123 937	-.004 493
.075	.124 186	-.004 873
.076	.124 430	-.005 242
.077	.124 668	-.005 602
.078	.124 900	-.005 952
.079	.125 128	-.006 295
.080	.125 351	-.006 629
.081	.125 685	-.006 955
.082	.125 782	-.007 273
.083	.125 990	-.007 583
.084	.126 195	-.007 887
.085	.126 395	-.008 183
.086	.126 591	-.008 474
.087	.126 783	-.008 757
.008	.126 971	-.009 035
.089	.127 156	-.009 307
.090	.127 337	-.009 573
.091	.127 514	-.009 834
.092	.127 688	-.010 089
.093	.127 859	-.010 340
.094	.128 027	-.010 585
.095	.128 191	-.010 826
.096	.128 353	-.011 063
.097	.128 511	-.011 295
.098	.128 667	-.011 523
.099	.128 820	-.011 747
.100	.128 970	-.011 967

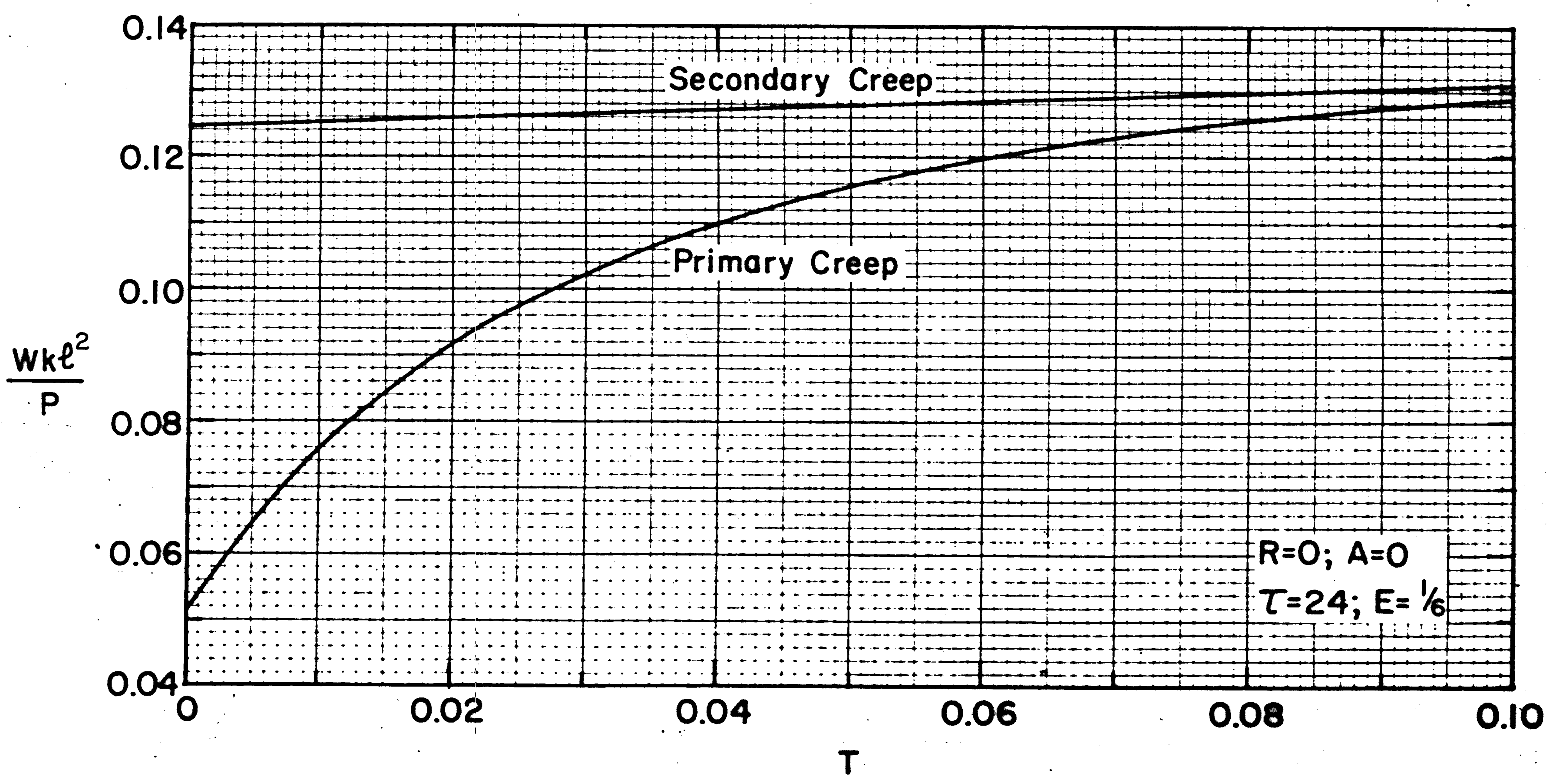

Figure 19. Primary creep deflections under a concentrated load.

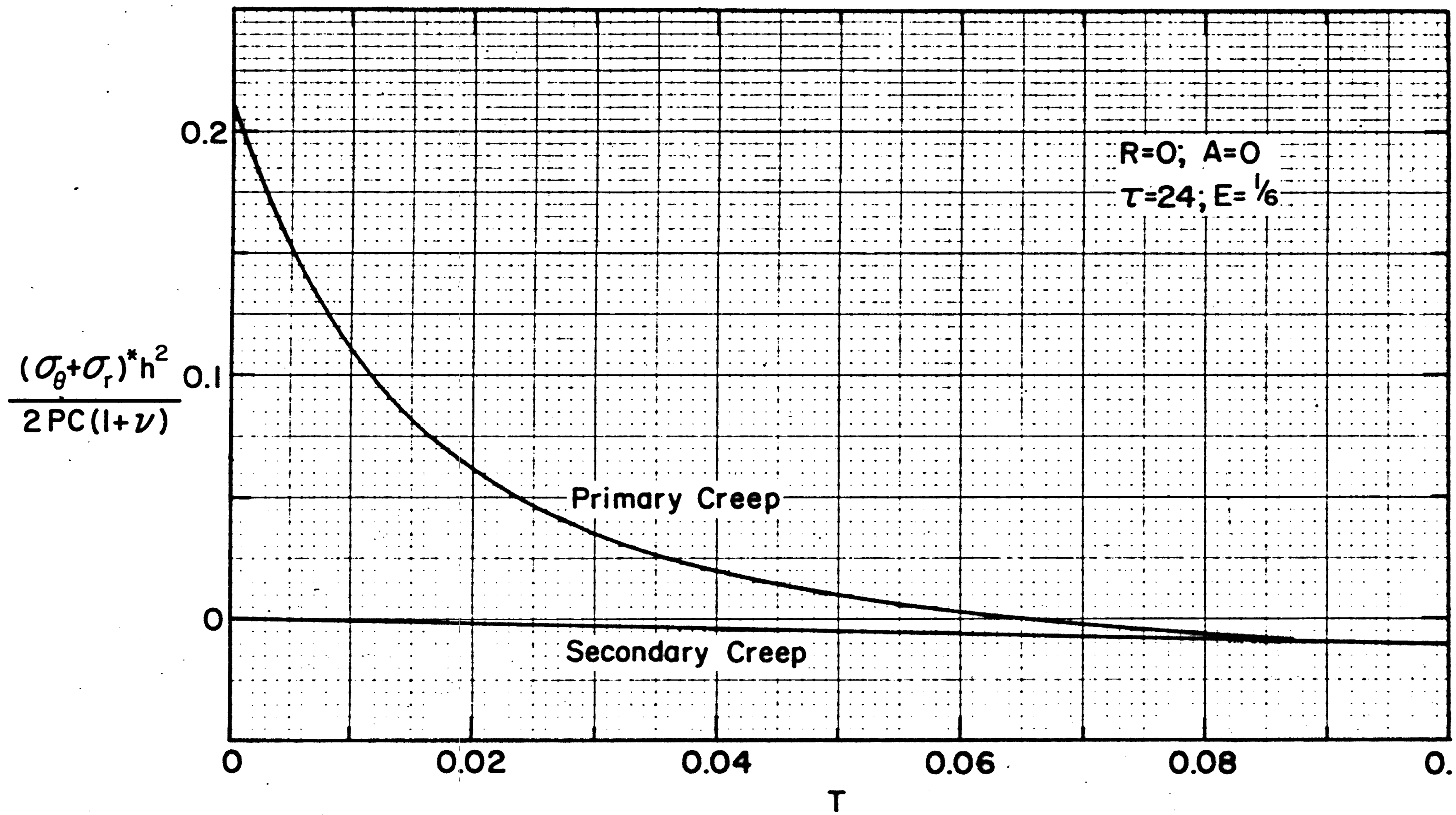

Figure 20. Primary creep stress $(\sigma_\theta+\sigma_r)^*$ under a concentrated load.

RAMP LOADS

Sometimes tests are performed with a load increasing linearly with time. Such a load is called a ramp load and we designate it by $P=\dot{P}t$ where $\dot{P}$ is a constant load rate. Frankenstein [32] and IAkunin [51] have both run tests in this manner. The reason for loading an ice sheet in this way is that heavy loads are easily produced by pumping water at a constant rate into a tank which is resting on the ice.

For this case the q in equation 7 becomes

$$q = \frac{\dot{P}t}{\pi a^2} \; H(a-r) \quad H(t), \tag{111a}$$

which when dividing by k and changing to dimensionless symbols, becomes

$$\frac{q}{k} = \frac{(\dot{P}\eta_o E_o) \; H(A-R)}{\pi k \ell^2 \; A^2} \; T \; H(T). \tag{111b}$$

This expression for q/k now becomes the right-hand side of equation 15. When the Laplace transform is taken, we obtain $1/s^2$ by means of equation 18c, rather than obtaining 1/s as before. The only other change in the Laplace-transformed equations is that P should be replaced with $\dot{P}\,\eta_o/E_o$.

Previously the Laplace-transformed equations had terms proportional to $P/(s+\alpha_i)$, whose inverse transform was $H(T)Pe^{-\alpha_i T}$. Here α_i means any of the roots from the previous solutions. Now we have transformed terms proportional to

$$\frac{\dot{P}\eta_o/E_o}{s(s+\alpha_i)}, \tag{112a}$$

which by partial fractions becomes

$$\frac{\dot{P}\eta_o}{E_o\alpha_i}\left(\frac{1}{s}-\frac{1}{s+\alpha_i}\right). \tag{112b}$$

The inverse transform is

$$H(T)\,\dot{P}t\,\frac{1-e^{-\alpha_i T}}{\alpha_i T}, \tag{113a}$$

and for the special case of $\alpha_i=0$, this becomes

$$H(T)\,\dot{P}t\,. \tag{113b}$$

Hence we conclude that the solution for the ramp function may be obtained from the previous integral solutions for the step function if P is replaced with $\dot{P}t$ and $e^{-\alpha_i T}$ is replaced with $(1-e^{-\alpha_i T})/(\alpha_i T)$.

As an example, let us consider secondary creep where $\alpha=1/(1+\beta^4)$. Equation 31 for the deflection becomes

$$\frac{wk\ell^2}{\dot{P}t}=\frac{H(T)}{2\pi}\int_0^\infty \frac{J_1(\beta A)}{\beta A/2}\left[1+(\alpha-1)\left(\frac{1-e^{-\alpha T}}{\alpha T}\right)\right] J_o(\beta R)\beta\, d\beta\,, \tag{114}$$

and the equations 43 for the stresses become

$$\frac{(\sigma_\theta+\sigma_r)h^2}{2\dot{P}tC(1+\nu)}=\frac{3H(T)}{2\pi}\int_0^\infty \frac{J_1(\beta A)}{\beta A/2}\,\frac{\alpha(1-e^{-\alpha T})}{\alpha T}\,J_o(\beta R)\,\beta^3 d\beta \tag{115a}$$

$$\frac{(\sigma_\theta-\sigma_r)h^2}{2\dot{P}tC(1-\nu)}=\frac{3H(T)}{2\pi}\int_0^\infty \frac{J_1(\beta A)}{\beta A/2}\,\frac{\alpha(1-e^{-\alpha T})}{\alpha T}\,\frac{J_1(\beta R)}{\beta R/2}\,\beta^3 d\beta - \frac{(\sigma_\theta+\sigma_r)h^2}{2\dot{P}tC(1+\nu)}\,. \tag{115b}$$

For R=0 and A=0, the deflection integrates to

$$\frac{wk\ell^2}{\dot{P}t} = \frac{1}{8}\ {}_1F_1(-\tfrac{1}{2},2,-T) = \frac{-1}{8}\sum_{k=0}^{\infty} \frac{(-T)^k}{k!(k+1)!}\ \frac{(2k-3)!!}{2^k}\ . \tag{116a}$$

For large T the asymptotic expansion gives

$$\frac{wk\ell^2}{\dot{P}t} = \frac{1}{2}\frac{\sqrt{T}}{\sqrt{\pi}} \sum_{k=0}^{\infty} \frac{-(2k-3)!!}{2^{2k}}\ \frac{(2k-5)!!}{k!T^k}\ , \tag{116b}$$

where $(-5)!! = \frac{1}{3}$.

For R=0 and A=0 the stress in equation 115a diverges. If we subtract the stresses at T=0 we have

$$\frac{(\sigma_\theta+\sigma_r)^* h^2}{2\dot{P}tC(1+\nu)} = \frac{3H(T)}{2\pi}\int_0^\infty \alpha[\frac{1-e^{-\alpha T}}{\alpha T} -1]\beta^3 d\beta\ , \tag{117a}$$

which integrates to

$$\frac{(\sigma_\theta+\sigma_r)^* h^2}{2\dot{P}tC(1+\nu)} = \frac{3H(T)}{8\pi}\ [\frac{1-T-e^{-T}}{-T} -E_1(T) - \log(T) - \gamma]. \tag{117b}$$

SECONDARY CREEP FOR REISSNER's PLATE THEORY

Ko[48] has solved the primary creep model for a floating ice sheet with Reissner's plate theory by using the same methods as in this paper. If the load radius A equals zero in his solutions, discontinuities appear in his solutions at R=0. In order to simplify this discussion, let us consider the two-element secondary creep model. The differential equation that must be solved is

$$D\nabla_r^4 w = (q-kw) - \psi^2 \ell^2 \nabla_r^2 (q-kw) \tag{118}$$

where $\psi^2 = (2-\nu)h^2 / [10(1-\nu)\ell^2]$. The procedure for solving this equation is the same as used before. Carrying out this procedure, the solution to this equation with the load uniformly distributed over an area of radius "a" is

$$w = \frac{P}{\pi k\ell^2} \int_o^\infty \frac{J_1(\beta A)}{\beta A} [1+(\alpha_5-1)e^{-\alpha_5 T}] J_o(\beta R)\, \beta d\beta , \tag{119a}$$

where

$$\alpha_5 = \frac{1+\psi^2\beta^2}{1+\psi^2\beta^2+\beta^4} . \tag{119b}$$

The vertical shear force per unit length is

$$Q = -\frac{P[R^2-(R^2-A^2)H(R-A)]}{2\pi\ \ell\ A^2\ R} + \frac{P}{\pi\ell}\int_o^\infty \frac{J_1(\beta A)}{\beta A} \{1+(\alpha_5-1)e^{-\alpha_5 T}\} J_1(\beta R)\ d\beta , \tag{120}$$

where H(R-A) is a step function. The stresses are given by

$$\frac{(\sigma_\theta+\sigma_r)h^2}{12(1+\nu)} = -\frac{P}{4\pi}\int_o^\infty \frac{J_1(\beta A)}{\beta A/2}[\alpha_5 e^{-\alpha_5 T}] J_o(\beta R)\beta^3 d\beta$$

$$+\frac{h^2}{10(1+\nu)\ell^2}[\frac{Q}{R}+\frac{\partial Q}{\partial R}] - \frac{\nu\psi^2\ell^2 (q-kw)}{(2-\nu)(1+\nu)}, \qquad (121a)$$

$$\frac{(\sigma_\theta-\sigma_r)h^2}{12(1-\nu)} = -\frac{P}{4\pi}\int_o^\infty \frac{J_1(\beta A)}{\beta A/2}[\alpha_5 e^{-\alpha_5 T}] [\frac{J_1(\beta R)}{\beta R/2} - J_o\beta R]\beta^3 d\beta$$

$$+\frac{h^2}{10(1-\nu)\ell^2}[\frac{Q}{R}-\frac{\partial}{\partial R}], \qquad (121b)$$

where the ice properties have been assumed to be uniform through the ice thickness.

The above integrals are convergent when $A\neq0$. When $A=0$ the deflection integral converges except at $R=0$. For $A=0$ the shear force Q and its derivative $\partial Q/\partial R$ are finite except at $R=0$. However, for $A=0$ the integrals in the stress equations diverge for any R. This is because the integrals in the stress equation are discontinuous at $A=0$. Therefore, to obtain the correct value, the integration should be performed before taking the limit as A approaches zero. If we subtract the elastic part for $T=0$, we see that we eliminate this divergence problem for any R. This shows that singularity is really associated with the elastic part. Vladimir Panc [73] has considered the elastic solution for a concentrated load. His method of solution was similar to that of D. Frederick [53] in that the general solution of the homogeneous differential equation was obtained. Knowing the boundary conditions at infinity, the limiting shear as "r" approaches zero, and that the slope equals zero at $r=0$, the solution was obtained. Panc then shows that the deflections, moments, and shear force have singularities at $r=0$ only.

A similar type of discontinuity occurs for $T=\infty$ in all the solutions of this paper. One must perform the integration before taking the limit as T approaches infinity. IAkunin [50] arrived at erroneous asymptotic values by letting $T=\infty$ before the integration was performed.

CONCLUSIONS AND RECOMMENDATIONS

In this paper a linear creep model for ice has been formulated which includes primary, secondary, and tertiary creep. The solution for the creep of a floating ice sheet using this model has been presented in integral form.

The solution is integrable for the results directly under a concentrated load. It has been shown how the distribution of the load is relatively unimportant for the time-dependent part of the solution. Therefore for the time-dependent part, a concentrated load may be assumed rather than a distributed load. The most important results have been tabulated and shown by figures in the report. Other results for specialized cases may be obtained by the same procedures. In general the results show that in the vicinity of the load, the deflections increase with time and the stresses decrease with time.

For practical application, the material constants must be known. A review of the creep tests that have been performed on floating ice sheets shows that the viscoelastic constants are not well established. However, reasonable estimates of the viscoelastic constants have been made from these tests and from other uniaxial creep tests. Those estimates may also include the effect of cracking and flooding of the ice, for which this theory does not account. In order to adequately verify the theory, better test data are needed. The theory can only predict creep up to the initial cracking of an ice sheet, similar to Wyman's solution for the elastic case. In order to predict beyond this time, the creep of a floating wedge may be a better mathematical model for the final breakthrough which offers a challenge for further work.

The results have shown that the stresses relax as time increases. I suspect that this statement would be true also if a nonlinear stress-strain relation would be used. This theory cannot explain why the ice sheet cracks after creeping for a period of time. In order to explain this we must know more about how the creep process affects the strength of the ice. With this additional information, the theory which has been presented here could be used to predict the initial crack in the ice sheet as a function of time. However, the theory can be used immediately to predict the deflection which is important when flooding of the ice sheet is undesirable.

This paper has dealt with the axially-symmetric creep problem in which there is only one coordinate distance and one load distribution length. The same methods would work in rectangular coordinates for loads distributed over rectangular areas provided the inverse Laplace transform can be obtained. However, in this case there are two coordinate distances and two load distribution lengths. The axial symmetry results depend upon fewer parameters, are more straightforward in their mathematical presentation, and are more readily visualized by the reader.

REFERENCES

1. Arnold D. Kerr, The bearing capacity of floating ice plates subjected to static or quasi-static loads, U.S. Army Cold Regions Research and Engineering Laboratory (CRREL) Research Report 333, Hanover, N.H. March 1975.

2. M. Hetényi, Beams and plate on elastic foundations and related problems, Applied Mechanics Review, Vol. 19, no. 2, p 95-102, Feb 1966.

3. F. Donald Haynes, Tensile strength of ice under triaxial stresses, CRREL Research Report 213, Dec 1973.

4. J. Langford and P.H. Francis, Strength of ice under multiaxial loading, Southwest Research Institute. Project 02-4071, Sep 1975.

5. Donald E. Nevel and F.D. Haynes, Interpretation of the tensile strength of ice under triaxial stress, CRREL Report 76-5 (in press).

6. Heinrich Hertz, Ueber das Gleichgewicht schwimmender elastischer Platten, Annalen der Physik und Chemie, Vol. 22, p 449-445, 1884.

7. August Föppl, Vorlesungen über technische Mechanik, vol. 5, p 112-130, B.G. Teubner, Leipzig, 1907.

8. Ferdinand Schleicher, Kreisplatten auf elastischer Unterlage, Julius Springer, Berlin, 1926.

9. G.N. Watson, A treatise on the theory of Bessel functions, p. 81, 2nd ed. 1944, Cambridge U. Press, London.

10. Max Wyman, Deflections of an infinite plate, Canadian Journal of Research, A. 28, p. 293-302, May 1950.

11. Donald E. Nevel, Tables of Kelvin Functions and their derivatives, U.S. Army Snow Ice Permafrost Research Establishment (SIPRE, now CRREL) Technical Report 67, June 1959.

12. H.M. Westergaard, Stresses in concrete pavements computed by theoretical analysis, Public Roads Vol. 7, no. 2, p. 25-35, April 1926.

13. A. Nadai, Die Biegungsbeanspruchung von Platten durch Einzelkräfte, Schweizerische Bauzeitung, Bd. 76, Nr 23, Dec 1920, p. 257-260; see also Die elastishen Platten, p. 308, Julius Springer, Berlin, 1925.

14. S. Woinowsky-Krieger, Der Spannungszustand in dicken elastischen Platten, Ingenieur-Archiv Band IV, Heft 3 and 4, 1933.

15. Donald E. Nevel, Concentrated loads on plates, CRREL Research Report 265, March 1970.

16. Hans Happel, Über das Gleichgewicht von elastischen Platten unter einer Einzellast, Mathematische Zeitschrift vol. 6, p. 203-218, 1920.

17. V. Lewe, Platten rechteckiger Grundrissteilung auf elastisch nachgiebiger Unterlage; Pilzdecke als Fundament. Bauingenieur, Vol. 3, p. 453-454, 1923.

18. H.M Westergaard, Om Beregning af plader paa elastisk underlag med saerligt henblik paa spørgsmaalet om spaendinger i Betonveje, Ingeriøren, nr. 42, p. 513-524, 1923.

19. Navier, Bull. Soc. Phil.-math., Paris 1823.

20. M Levy, Comp. rend. vol. 129, p. 535-539, 1899.

21. R.K. Livesley, Some notes on the mathematical theory of a loaded elastic plate resting on an elastic foundation, Quart. Journ. Mech. and Applied Math, Vol. VI, pt 1, p. 32-44, 1953.

22. Arnold D. Kerr, Elastic plates on a liquid foundation, Proc. Amer. Soc. of Civil Engineers, vol. 89, EM. 3, no. 3542, June 1963 p 59-71.

23. M.S. Skarlatos, Deflections and stresses in concrete pavements of airfields with continuous elastic joints, Contract W-33-107-eng-4240 to Ohio River Division Lab., June 1949.

24. G.S. Shapiro, Izgib polubeskonechnoi plity, lezhashchei na uprugom osnovanii, (Deflection of a semi-infinite plate on an elastic foundation), Prikladnaia mathematika i mekhanika Tom VIII 1943, Institut mechaniki, Akademiia Nauk. SSSR, see also SIPRE, Translation 48, January 1955.

25. Donald E. Nevel, A semi-infinite plate on an elastic foundation, CRREL Research Report 136, March 1965.

26. H.J. Fletcher and C.J. Thorne, Thin rectangular plates on elastic foundation, J. of Applied Mechanics, Vol. 19, p. 361-368, Sep 1952.

27. Donald E. Nevel, The narrow infinite wedge on an elastic foundation, SIPRE Technical Report 56, July 1958.

28. Donald E. Nevel, The narrow free infinite wedge on an elastic foundation, CRREL Research Report 79, July 1961.

29. Donald E. Nevel, The general solution of a wedge on an elastic foundation, CRREL Research Report 227, Nov 1968.

30. D.F. Panfilov, Eksperimental´nye issledovaniia gruzopodbemnosti ledianogo pokrova (Experimental investigation of the carrying capacity of an ice cover), Izvestiia Vsesouiznogo Nauchno-Issledovastel´skogo Instituta Gidrotechniki, Vol. 64, p. 101-115, 1960.

31. Donald E. Nevel, The ultimate failure of a floating ice sheet. International Association of Hydraulic Research. Ice symposium, Leningrad, 1972.

32. G.E. Frankenstein, Strength of ice sheets, in Ice pressures against structures, National Research Council of Canada Technical Memorandum No. 92, p. 79-87, March 1968.

33. Anders Johannson, Försök med armerade betongplattor pa elastiskt underlag, Betong Vol. 32, No. 3, p. 187-209, 1947.

34. G.G. Meyerhof, Bearing capacity of floating ice sheet, Proc. of Amer. Soc. of Civil Engineers, EM5 Oct 1960, p. 113-145.

35. Max D. Coon and M.M. Mohaghegh, Plastic analysis of coulomb plates and its application to the bearing capacity of sea ice, Scientific Report to the Office of Naval Research, Dept. of Atmospheric Sciences, University of Washington, 1972.

36. D.L. Holl, Dynamic loads on thin plates on elastic foundations. Applied Mathematics Symposium of the American Mathematical Society, Vol. 3, p. 107-116, 1950.

37. James T. Wilson, Coupling between moving loads and flexural waves in floating ice sheets. SIPRE Report 34, Sept 1955.

38. James T. Wilson, Moving loads on floating ice sheets, U. of Michigan Research Inst. project 2432, Ann Arbor, Michigan, July 1958.

39. A.G. Greenhill, Wave motion in hydrodynamics, American Journal of Mathematics, vol. IX, p. 62-112, 1887.

40. Dmitrii E Kheisin, Peremeshchenie nagruzki po uprugoi plastinke, plavaiushchei na poverkhnosti edealnoi zhidkosti (Moving loads on an elastic plate, floating on the surface of an ideal liquid), Mekhanika i mashinostroenie, no. 1, p. 178-180, 1963.

41. Dmitrii E. Kheisin, Dinamika ledianogo pokrova (Dynamics of the ice cover), Gidrometeorologicheskoe Izd-vo, Leningrad. 1967; see also CRREL Draft transtation 73.

42. Donald E. Nevel, Moving loads on a floating ice sheet, CRREL Research Report 261, May 1970.

43. Dmitrii E. Kheisin, Nestatsionarnaia zadacha o kolebaniiakh beskonechnoi uprugoi plastinki, plavaiushchei na poverkhnosti idealnoi zhidkosti (Unstationary problem of vibration of an infinite plate floating on the surface of an ideal liquid), Mekhanika i mashinostroenie, No. 1, p. 87-90, 1962.

44. Donald E. Nevel, Vibration of a floating ice sheet, CRREL Research Report 281, August 1970.

45. Herbert Reismann and Yu-Chung Lee, Dynamics of a floating ice sheet, Hydronautics, p. 108-111, April 1968.

46. Dmitrii E. Kheisin, K zadache uprugo-plasticheskogo izgiba ledianogo pokrova (The problem of elastic-plastic deflection of an ice sheet), Leningrad. Arkticheskii i Antarkticheskii nauchno-issledovatel'skii institut. Trudy 1964. Vol. 267. p. 143-149.

47. Donald E. Nevel, Time dependent deflection of a floating ice sheet, CRREL Research Report 196, July 1966.

48. Donald H. Garbaccio, Creep of floating ice sheet, Naval Civil Engineering Laboratory Report No. CR-67.025, Port Hueneme, Calif, April 1967.

49. Donald H. Garbaccio, Creep of floating ice sheets computer calculations, Naval Civil Engineering Laboratory Report No. CR-69014, Port Hueneme, Calif, Dec 1968.

50. A.E. IAkunin, K voprosu ob izgibe ledianogo prokrova s uchetom viazkikh svolstv l'da (Calculation of ice-cover bending allowing for viscous properties of ice) Novosibirskiy Institut Inzhenerov Zheleznodorozhnogo Transporta, Trudy, Transactions, Vol. 79, pp. 72-82, 1968; (See also CRREL Draft translation 425).

51. A.E. IAkunin, Issledovanie vliigniia vremeni deistviia nagruzki na nesushchuiu sposobnost ledianogo pokrova (Investigation of the influence of time of working load on bearing capacity of ice sheet), Novosibirskiy Institut Inzhenerov Zheleznodorozhnogo Transporta, Specialty 01.022, Resistance of Materials and Structural Mechanics. p. 1-22, 1970.

52. Paul M. Naghdi and J.C. Rowley, On the bending of axially symmetric plates on elastic foundations, Proc. 1st Midwestern Conf. on Solid Mechanics, p. 119-123, 1953.

53. Daniel Frederick, On some problems in bending of thick circular plates on an elastic foundation, J. of Applied Mechanics, June 1956, p. 195-200.

54. Daniel Frederick, Thick rectangular plates on an elastic foundation, Proc. of Amer. Soc. of Civil Engineers, Vol. 81, paper no. 818, Oct 1955.

55. Michael G. Katona, Ice engineering: viscoelastic finite element formulation, Naval Civil Engineering Laboratory Technical Report R803, Port Hueneme, Calif., Jan. 1974.

56. Kennon D. Vaudrey and M.G. Katona, Viscoelastic finite element analysis of sea ice sheets, International Association of Hydraulic Research, Third International Symposium on ice problems. CRREL Hanover, NH, Nov. 1975.

57. Kolumban Hutter, A general nonlinear viscoelastic plate theory and its application to floating ice, Acta Mechanica Vol. 21, p. 313-327, 1975.

58. Shiou-San Kuo, Stress and time effect on the creep rate of polycrystalline ice, Ph.D. Thesis, Michigan State University, 1972.

59. H.H.G. Jellinek and R. Brill, Viscoelastic properties of ice, Journal of Applied Physics, Vol. 27, No. 10, p. 1198-1209 1956.

60. P.A. Sumskij, Über das fliessgesetz in polykristallinem Eis, Polarforschung, Vol. 44, No. 2, p. 105-116, 1974.

61. B. Van Der Pol and H. Bremmer, Operational calculus based on the two-sided Laplace integral, 2nd Ed. Cambridge University Press. London, 1959.

62. Ian H. Sneddon, Fourier Transforms, McGraw-Hill, New York, 1951.

63. I.M. Longman, A short table of $\int_x^\infty J_0(t)\, t^{-n}\, dt$ and $\int_x^\infty J_1(t)\, t^{-n}\, dt$, Math. Tables and Aids to Computation, Vol. 13, p. 306-311, 1959.

64. M. Abramowitz and J.A. Stegun, Editors, Handbook of Mathematical functions, National Bureau of Standards Applied Mathematics Series 55, 1964.

65. Harry Bateman, Table of integral transforms, Vol. 1, McGraw-Hill, New York, 1954.

66. Shunsuke Takagi and D. Nevel, Mathematical study of the viscoelastic deformation of a floating ice sheet under a circular load, CRREL Technical Note, Oct 1974.

67. John Burdick, Tensile creep-rupture of ice, Third international conference on port and ocean engineering under Arctic condtions, p. 193-194, University of Alaska, 1975.

68. D.F. Panfilov, k raschety gruzpodbemnosti ledianogo pokrova pri stoianke gruzov na L'dy (On the determination of the carrying capacity of an ice cover for loads of long duration), Izvestiia Vysshikh Uchebnykh zavedeniy Ministerstva Vysshego i Srednego Spetsial'nogo Obrazovaniya SSSR, No. 6, p. 47-57, 1961.

69. Marlin Sundberg-Falkenmark, The load bearing capacity of ice, the Swedish Institute of Meteorology and Hydrology, Hydrology Series No. 1, Stockholm 1963.

70. Ivor Hawkes and M. Mellor, Deformation of ice under uniaxial stress, Journal of Glaciology Vol 11, No. 61, p. 103-131, 1972.

71. Malcolm Mellor and R. Testa, Creep of ice under low stress, Journal of Glaciology Vol 8, No. 52, p. 147-152, 1969.

72. H.A. Hobbs and W.D. Kingery, Long-time tests of sea ice sheet deformation, in Air Force Surveys in Geophysics No. 145, Summary Report-Project Ice Way, W.D. Kingery, editor, May 1962.

73. Vladimiŕ Panc, Theories of elastic plates, Noordhoff International Publishing, Leydon, Netherlands, 1975.